



DTIC
ELECTE
JAN 05 1995
S G D

OPTIMIZATION OF A NUTATION DAMPER
ATTACHED TO A SPIN-STABILIZED SATELLITE

THESIS

Brady P. Hauboldt, 2nd Lieutenant, USAF

AFIT/GSO/ENY/94D-2

Acc
NTIS
DTIC
GPO

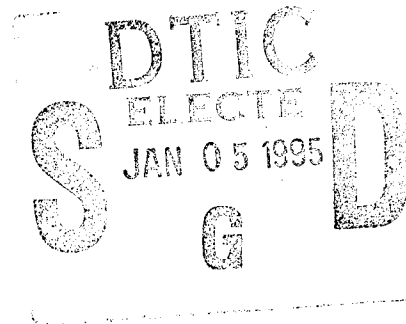
DEPARTMENT OF THE AIR FORCE
AIR UNIVERSITY
AIR FORCE INSTITUTE OF TECHNOLOGY

19950103 076

Wright-Patterson Air Force Base, Ohio

DISTRIBUTION STATEMENT A

Approved for public release;
Distribution Unlimited



OPTIMIZATION OF A NUTATION DAMPER
ATTACHED TO A SPIN-STABILIZED SATELLITE

THESIS

Brady P. Hauboldt, 2nd Lieutenant, USAF

AFIT/GSO/ENY/94D-2

Accession For	
NTIS CRA&I	<input checked="" type="checkbox"/>
DTIC TAB	<input type="checkbox"/>
Unannounced	<input type="checkbox"/>
Justification _____	
By _____	
Distribution / _____	
Availability Codes	
Dist	Avail and/or Special
A-1	

DTIC QUALITY INSPECTED 8

OPTIMIZATION OF A NUTATION DAMPER ATTACHED TO A SPIN-
STABILIZED SATELLITE

THESIS

Presented to the Faculty of the School of Engineering
of the Air Force Institute of Technology

Air University

In Partial Fulfillment of the
Requirements for the Degree of
Master of Science in Space Operations

Brady P. Hauboldt, B.S.

Second Lieutenant, USAF

December 1994

Approved for public release; distribution unlimited

Acknowledgments

Sincere thanks to Dr. Christopher Hall who has provided me with the clues I've needed to complete this thesis. Thanks also to Captain Nathan Titus of the Phillips Lab for his interest in my work. Most importantly, thanks to Jennifer for pushing me to keep going when I felt as if I'd had enough.

Table of Contents

	Page
Acknowledgments	i
Table of Contents	ii
List of Figures	iv
List of Tables	v
List of Symbols	vi
Abstract	vii
I. Introduction	1
Background	1
History	3
Problem Statement	4
II. Formulation	6
Equations of Motion	6
Non-Dimensionalization	8
Linearization of Equations of Motion	10
Stability Criteria	11
III. Damping Effects	13
Eigenvalue and Eigenvector Analysis	13
Independent Parameter Effects	16
IV. Optimization Problem	24

Maximization of the Damping Rate.....	24
Minimization Methods.....	25
Effects of Varying the Damping Coefficient.....	26
Effects of Varying the Spring Constant.....	28
Effects of Varying the Location of the Spring-Mass-Damper.....	29
V. Comparisons to a Classical Tuning Method.....	33
Classical Nutation Damper Design.....	33
Actual Results.....	35
VI. Conclusion.....	41
Appendix A: Sample MatLab Code.....	44
Appendix B: Supportive Plots.....	48
Bibliography.....	54
Vita.....	57

List of Figures

	Page
Figure 1, System Model.....	7
Figure 2, Damping Over Time and Eigenvalues for Damping Types	14
Figure 3, General Variation of Eigenvalues	17
Figure 4, Effects of the Spring-Mass-Damper Placement, b	19
Figure 5, Effects of the Damping Coefficient, c	20
Figure 6, Effects of the Spring Constant, k	21
Figure 7, Effects of the Moments of Inertia, I_1 and I_3	22
Figure 8, Effects of the Mass Fraction, ϵ	23
Figure 9, Real Eigenvalue Part Dependence Upon the Damping Coefficient, c	27
Figure 10, Real Eigenvalue Parts Effects Based Upon the Spring Constant, k	28
Figure 11, Damping Coefficient and Spring Constant Relation for Minimum Reals.....	29
Figure 12, Minimum Real Eigenvalues for a Practical Range of b	30
Figure 13, Minimum Real Eigenvalues for $b = \{0.25, 0.50, 0.75, 1, 2, 3\}$	31
Figure 14, Apparent Eigenvalue Equality at Optimum.....	34
Figure 15, Spring Constant/Damping Coefficient Relationships.....	35
Figure 16, Comparison of Minimum Attainable Eigenvalues	36
Figure 17, Increased Damping Rates for Optimal Parameter Selection	37
Figure 18, Response of Real Eigenvalue Parts for Tuning Methods.....	38
Figure 19, Damping Coefficient and Spring Constant Comparison for Tuning Methods..	39

List of Tables

	Page
Table 1, List of System Parameters	16

List of Symbols

\mathcal{R}	Rigid Body
\mathcal{P}	Spring-Mass-Damper
\mathbf{r}_p	Position vector of mass particle
m_p	Particle mass
m	System mass
\mathbf{n}	Axial direction of spring-mass-damper
x	Displacement of mass particle from equilibrium
\dot{x}	Velocity of mass particle
c	Damping coefficient
k	Spring constant
b	Distance to the spring-mass-damper
ϵ	Mass fraction ($\epsilon' = 1 - \epsilon$)
\mathbf{e}	Coordinate frame
\mathbf{p}_p	Linear momentum vector of the mass particle
p_n	Linear momentum of mass particle in the \mathbf{n} direction
\mathbf{c}	1 st moment of inertia of the system
\mathbf{J}	2 nd moment of inertia of the system
$\boldsymbol{\omega}$	Angular velocity vector
k_g	Radius of gyration
\mathbf{v}_o	Linear velocity of system
\mathbf{h}	Angular momentum vector
\mathbf{I}	Moment of inertia of the rigid body
k_{crit}	Minimum stable value for k
\mathbf{Y}_{EQ}	Equilibrium position vector
\mathbf{Z}	Position vector
RB	Rigid body
SMD	Spring-Mass-Damper
c_{crit}	Critically damped value for c
ω_n	Rigid body natural frequency (uncoupled)
ω_d	Spring-mass-damper damped frequency (uncoupled)
σ	Real eigenvalue part

Abstract

This study uses linearized equations of motion for a rigid body with an attached spring-mass-damper to maximize the decay rate of a satellite's coning motion. An analysis of the numerical eigenvalues is presented which leads to an optimal relationship between relevant parameters--damper placement, spring constant, damping coefficient, system moments of inertia, and damper mass fraction. The coupled system's eigenvalues do not provide truly critical damping, thus the real eigenvalue parts are minimized in order to achieve damping which requires the minimum amount of time. A comparison between this optimal design method and a classical method concludes a noticeable improvement in damping performance for optimized systems.

I. Introduction

Background

Since the launch of the first satellite in 1957 by the Soviet Union, dynamicists have investigated the motion of rigid bodies as they apply to spin-stabilized satellites. Most satellites rely upon their ability to fix an axis toward earth in order to accomplish such missions as communications and reconnaissance. A spin-stabilized satellite accomplishes this through a large inherent angular momentum, leaving perturbing moments relatively small and ineffective. The need for effective satellite attitude control was fully realized with the failure of the United States' Explorer I.

The first major tenet in the analysis of the dynamics of rotating bodies concludes that *a rigid body spun about an intermediate moment of inertia principal axis is unstable* (17:484). Adding energy dissipation ensures that *only rotation about the principal axis of maximum inertia is stable* (17:485). This was the case of the Explorer I satellite, intended to spin about its longitudinal (minor) axis. Long, flexible antennas acted as the energy dissipation mechanism, causing a coning angle of approximately 60 degrees within its first orbit (17:484). With this failure, designers turned their attention to the design of nutation dampers as a passive means of improving attitude control about the axis of maximum moment of inertia.

In modern practice, many satellites use advanced spin-stabilization methods such as dual-spin, momentum wheels, or thrust control. Shifts toward simpler, less costly satellites may again utilize passively damped spin-stabilized systems. Nutation dampers,

similar in design but different in orientation to precession dampers, are devices which increase energy dissipation, tuned to return the satellite to a state of pure spin (25:132). These passive damping elements often resemble a spring-mass-damper system in a fluid-filled tube and are desirable since they do not rely on complicated control systems or use precious fuel (25:133). Other damper types include the viscous ring and the two degree of freedom spherical pendulum. The addition of a nutation damper assists a spin-stabilized satellite by damping out coning motions caused by booster separation (14:543), docking, crew motions (23:1221), eddy-currents, or magnetic torques (26:2169). By selecting proper components of the nutation damper, it can efficiently control the attitude of a spin-stabilized satellite. A classical design method involves tuning the damper only to the rigid body's natural frequency, disregarding coupled effects (6:166, 20:298, 21:219, 11:52). In an uncoupled model, the spring-mass-damper has no effect upon the motion of the rigid body, an assumption that should be avoided.

A primary area of interest in the design of nutation dampers is the relationship between the spring-mass-damper parameters. It is the critical damping coefficient which ensures the maximum energy dissipation in the minimal amount of time. An underdamped system will eventually damp out, but will require oscillation of the system over a relatively long period of time. Overdamped systems will directly damp out, but at a very slow rate. Thus, for satellite applications, it is desirable to select a spring-mass-damper which will minimize the amount of time necessary to damp out oscillations.

History

The failure of the Explorer I satellite in the late 1950s may have prompted much of the work of the following decade. The effectiveness of nutation dampers in reducing coning motions was well known, however damper design was often deficient. In 1962, dynamicist W. R. Haseltine concluded that nutation damper design was “very much a cut-and-try proposition” (14:543). Stability analyses led the effort, often limited in scope by computer capability. By 1964, dynamically stable systems were being designed, but the determination of the degree of stabilization was not as straightforward (24:588). Due to the nonlinearities of this problem, typical stability analyses were not exact. Approximations, equation of motion simplifications, and computer simulation helped analysts study the satellite model.

Efforts were primarily aimed at developing a device which maximized the amount of energy dissipated per pound of weight (21:219). Several researchers studied the effects of multiple dampers (13:545, 19:848) and other damper types (1:456, 2:50, 3:1, 4:383, 23:1221) to include both viscous ring and pendulum dampers. Viscous ring dampers, in the case of the *Telstar* satellite, incorporate two curved aluminum tubes filled with neon gas at one atmosphere of pressure. Each tube contains a single tungsten ball which dissipates energy as heat while moving through the viscous gas (26:2182). The pendulum damper acts as a combined precession and nutation damper due to its two-direction degree of freedom (2:50). In the Orbiting Solar Observatory, a pendulum damper is used

which has a circular steel arm, spherical zinc bob, and silicone damping fluid (11:51). A third type of damper, the classic ball-in-tube, simplifies the analysis and has also been studied (6:165).

Problem Statement

The equations of motion of a rotating body with an attached spring-mass-damper have been previously developed (15:65), but much of the analysis was limited to steady state motion of the system or approximate solutions. Other works have investigated the transient motion of the system and defined stable motion as functions of the spring's stiffness (7:3, 8:25). Several studies have proven that tuning the spring-mass-damper to the satellite's natural frequency improves the system response (6:165, 11:52, 20:298, 21:219), but few have determined an optimal solution.

This study first reviews the derivation of the equations of motion of a rigid body with an attached ball-in-tube damper in general form. Next, a summary of the non-dimensionalizations (8:12) leaves the equations of motion in a more usable state. Linearization of the equations of motion about an equilibrium reduces the equations of motion into their final form. Stability of the system and its importance are discussed.

Using the linearized equations of motion of the system, an analysis is conducted of the eigenvalues and eigenvectors. Two pairs of eigenvalues for this fourth order system are used to determine the type and degree of damping each parameter affects. An eigenvector analysis verifies the high degree of coupling between the spring-mass-damper and rigid body, indicating that uncoupled tuning methods are not entirely sufficient.

After the initial discussion of parameters and damping, an optimization scheme is introduced which endeavors to find the parameter set which induces minimum damping time. The system's real eigenvalue parts are used as the minimized parameter in order to

induce the greatest system stability. Lastly, this optimal, exact solution method is compared to historical tuning techniques which assume a physically uncoupled system.

II. Formulation

Several dynamicists have developed equations of motion for rigid bodies with attached spring-mass-dampers. However, many used approximations or made assumptions in order to avoid nonlinearities during the development of the equations of motion. This study uses exact equations of motion for a rigid body with an attached ball-in-tube spring-mass-damper. Next, the parameters are non-dimensionalized (8:12-15). The resulting equations are highly nonlinear and require linearization about a desirable equilibrium solution. The stability criteria are discussed and the importance of designing an inherently stable system is emphasized. This chapter provides an overview of the development of the equations of motion used in further analysis.

Equations of Motion

In order to complete an analysis of the system, the equations of motion must first be developed. An overview of these relations is presented which is most applicable to the current analysis. The majority of this derivation stems from Hughes' text (15:62-64), while additional refinement was accomplished by Chinnery and Hall in their paper (7:2). Both are recommended to the interested reader.

A schematic of the system model is provided in Figure 1, showing the rigid body, \mathcal{R} , and attached point mass, ρ . Within the spring-mass-damper (nutration damper), the point mass, m_ρ , is allowed to move freely along the axial direction, \mathbf{n} . This motion is governed by the damping coefficient, c , and the spring constant, k . The particle's motion within the spring-mass-damper provides the energy dissipation mechanism necessary to stabilize the nominal spin about \mathbf{e}_2 .

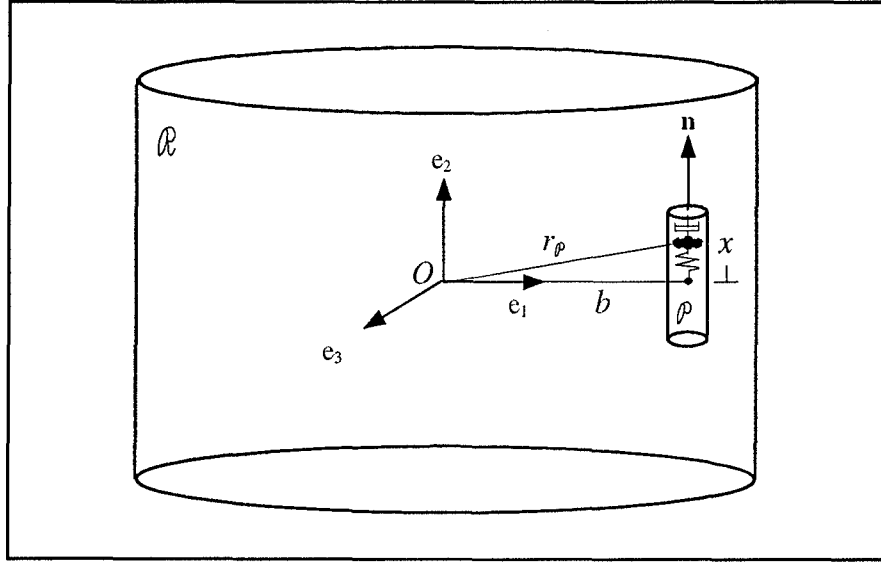


Figure 1, System Model

Hughes develops the vectorial equations of motion by first defining the linear momenta of the rigid body, \mathbf{p}_R , and the spring-mass-damper, \mathbf{p}_ρ

$$\mathbf{p}_R = \int_R (\mathbf{v} + \boldsymbol{\omega} \times \mathbf{r}) dm = m_R \mathbf{v} + \boldsymbol{\omega} \times \mathbf{c}_R \quad (1)$$

$$\mathbf{p}_\rho = m_\rho (\mathbf{v} + \boldsymbol{\omega} \times \mathbf{r}_\rho + \dot{x} \mathbf{n})$$

The total linear momentum of the system is then

$$\mathbf{p} = \mathbf{p}_R + \mathbf{p}_\rho = m \mathbf{v} - \mathbf{c} \times \boldsymbol{\omega} + m_\rho \dot{x} \mathbf{n} \quad (2)$$

Additionally, we are interested in the component of \mathbf{p}_ρ along the damper's axial direction, denoted by p_n

$$p_n = \mathbf{n} \cdot \mathbf{p}_\rho = m_\rho (\mathbf{n} \cdot \mathbf{v} - \mathbf{n} \times \mathbf{b} \cdot \boldsymbol{\omega} + \dot{x}) \quad (3)$$

The angular momentum is next defined as

$$\mathbf{h}_R = \int_R \mathbf{r} \times (\mathbf{v} + \boldsymbol{\omega} \times \mathbf{r}) dm = \mathbf{c}_R \times \mathbf{v} + \mathbf{J}_R \cdot \boldsymbol{\omega} \quad (4)$$

$$\mathbf{h} = \mathbf{h}_R + \mathbf{r}_\rho \times \mathbf{p}_\rho = \mathbf{c} \times \mathbf{v} + \mathbf{J} \cdot \boldsymbol{\omega} + m_\rho \dot{x} \mathbf{b} \times \mathbf{n}$$

where \mathbf{c} and \mathbf{J} are the first and second moments of inertia of the system about the origin.

They are

$$\begin{aligned}\mathbf{c} &= \mathbf{c}_R + m_\rho \mathbf{r}_\rho \\ \mathbf{J} &= \mathbf{J}_R + m_\rho \left(r_\rho^2 \tilde{\mathbf{I}} - \mathbf{r}_\rho \mathbf{r}_\rho \right)\end{aligned}\quad (5)$$

The dimensional equations of motion as derived by Hughes (15:64) are

$$\begin{aligned}\mathbf{p} &= m\mathbf{v}_o - \mathbf{c}^\times \boldsymbol{\omega} + m_\rho \dot{\mathbf{x}} \mathbf{n} \\ \mathbf{h} &= \mathbf{c}^\times \mathbf{v}_o + \mathbf{J} \boldsymbol{\omega} + m_\rho \dot{\mathbf{x}} \mathbf{b}^\times \mathbf{n} \\ p_n &= m_\rho \left(\mathbf{n}^T \mathbf{v}_o - \mathbf{n}^T \mathbf{b}^\times \boldsymbol{\omega} + \dot{\mathbf{x}} \right) \\ \dot{\mathbf{p}} &= -\boldsymbol{\omega}^\times \mathbf{p} \\ \dot{\mathbf{h}} &= -\boldsymbol{\omega}^\times \mathbf{h} - \mathbf{v}_o^\times \mathbf{p} \\ \dot{p}_n &= m_\rho \boldsymbol{\omega}^T \mathbf{n}^\times \left(\mathbf{v}_o - \mathbf{r}_\rho^\times \boldsymbol{\omega} \right) - c\dot{\mathbf{x}} - kx\end{aligned}\quad (6)$$

Note that the superscript “ \times ” denotes the skew symmetric matrix of the listed vector. It is a simplified method for computing the cross product through matrix multiplication. For example, the angular velocity, $\boldsymbol{\omega}$, crossed with another vector can be computed using $\boldsymbol{\omega}^\times$

$$\boldsymbol{\omega}^\times = \begin{bmatrix} 0 & -\omega_3 & \omega_2 \\ \omega_3 & 0 & -\omega_1 \\ -\omega_2 & \omega_1 & 0 \end{bmatrix}\quad (7)$$

Non-Dimensionalization

The equations of motion are non-dimensionalized at this point to simplify later analysis (7:2). The first step is to assume that there are no external forces or torques, thus linear and angular momenta are constant. The dimensional variables (denoted by a superscript star) as functions of their dimensionless counterparts are found on the following page.

$$\begin{aligned}
p^* &= \frac{h^* m^* b^*}{I_2^*} p & v_o^* &= \frac{h^* b^*}{I_2^*} v_o & t^* &= \frac{I_2^*}{h^*} t \\
h^* &= h^* h & \omega^* &= \frac{h^*}{I_2^*} \omega & \mathbf{b}^* &= b^* \mathbf{b} \\
p_n^* &= \frac{h^* m^* b^*}{I_2^*} p_n & \dot{x}^* &= \frac{h^* b^*}{I_2^*} \dot{x} & \mathbf{J}^* &= I_2^* \mathbf{J} \\
& & x^* &= b^* x & &
\end{aligned} \tag{8}$$

The dimensionless parameters are next defined as

$$\begin{aligned}
\varepsilon &= \frac{m_p^*}{m^*} & c &= \frac{c^* I_2^*}{m^* h^*} \\
b &= \frac{m^* b^{*2}}{I_2^*} & k &= \frac{k^* I_2^{*2}}{m^* h^{*2}}
\end{aligned} \tag{9}$$

$$\varepsilon' = 1 - \varepsilon \tag{10}$$

The parameter b characterizes the distance from the origin to the position of the nutation damper (Figure 1) and is closely related to the radius of gyration, k_g , about the e_2 axis since (7:2)

$$I_2^* = m^* k_g^{*2} \tag{11}$$

The dimensionless form of the moment of inertia matrix is

$$\mathbf{J} = \begin{bmatrix} I_1 + \varepsilon b x^2 & -\varepsilon b x & 0 \\ -\varepsilon b x & 1 & 0 \\ 0 & 0 & I_3 + \varepsilon b x^2 \end{bmatrix} \tag{12}$$

and the final non-dimensional equations of motion are

$$\begin{aligned}
\mathbf{p} &= \mathbf{v}_o - \frac{1}{b} \mathbf{c}^{\times} \omega + \varepsilon \dot{x} \mathbf{n} \\
\mathbf{h} &= \mathbf{c}^{\times} \mathbf{v}_o + \mathbf{J} \omega + \varepsilon b \dot{x} \mathbf{b}^{\times} \mathbf{n} \\
p_n &= \varepsilon (\mathbf{n}^T \mathbf{v}_o - \mathbf{n}^T \mathbf{b}^{\times} \omega + \dot{x}) \\
\dot{\mathbf{p}} &= -\omega^{\times} \mathbf{p} \\
\dot{\mathbf{h}} &= -\omega^{\times} \mathbf{h} - \mathbf{v}_o^{\times} \mathbf{p} \\
\dot{p}_n &= \varepsilon \omega^T \mathbf{n}^{\times} (\mathbf{v}_o - \mathbf{r}_p^{\times} \omega) - c \dot{x} - k x
\end{aligned} \tag{13}$$

Without external forces, linear momentum is conserved and $\mathbf{p} = \mathbf{0}$ is assumed without loss of generality. Thus \mathbf{v}_o and $\boldsymbol{\omega}$ are eliminated from the above equations and a fifth order, non-dimensional system is obtained

$$\begin{aligned} \dot{\mathbf{h}} &= \mathbf{h}^\times \mathbf{K}^{-1} \mathbf{L} \\ \dot{p}_n &= -\varepsilon \mathbf{L}^T \mathbf{K}^{-1} \mathbf{n}^\times \left[(\varepsilon' \mathbf{x} \mathbf{n} + \mathbf{b})^\times \mathbf{K}^{-1} \mathbf{L} + \varepsilon \dot{\mathbf{x}} \mathbf{n} \right] - c \dot{\mathbf{x}} - k \mathbf{x} \\ \dot{\mathbf{x}} &= \frac{p_n + \mathbf{n}^T \mathbf{b}^\times \mathbf{K}^{-1} \mathbf{h}}{\varepsilon' + \varepsilon \mathbf{b} \mathbf{n}^T \mathbf{b}^\times \mathbf{K}^{-1} \mathbf{b}^\times \mathbf{n}} \end{aligned} \quad (14)$$

where

$$\begin{aligned} \mathbf{L} &= \mathbf{h} - \varepsilon \mathbf{b} \dot{\mathbf{x}} \mathbf{b}^\times \mathbf{n} \\ \mathbf{K}^{-1} &= \begin{bmatrix} \frac{1}{D_1} & \frac{\varepsilon \mathbf{b} \mathbf{x}}{D_1} & 0 \\ \frac{\varepsilon \mathbf{b} \mathbf{x}}{D_1} & \frac{D_2}{D_1} & 0 \\ 0 & 0 & \frac{1}{D_3} \end{bmatrix} \\ D_1 &= I_1 + \varepsilon \mathbf{b} (\varepsilon' - \varepsilon \mathbf{b}) \mathbf{x}^2 \\ D_2 &= I_1 + \varepsilon \varepsilon' \mathbf{b} \mathbf{x}^2 \\ D_3 &= I_3 + \varepsilon \varepsilon' \mathbf{b} \mathbf{x}^2 \end{aligned} \quad (15)$$

Linearization of Equations of Motion

To analyze the system stability, a linear set of equations must be available. Since the equations of motion are highly nonlinear, they are linearized about a known, equilibrium solution corresponding to pure spin about the \mathbf{e}_2 axis:

$$\mathbf{Y}_{EQ} = \begin{bmatrix} h_1 \\ h_2 \\ h_3 \\ p_n \\ \mathbf{x}_{EQ} \end{bmatrix} = \begin{bmatrix} 0 \\ 1 \\ 0 \\ 0 \\ 0 \end{bmatrix} \quad (16)$$

This solution provides a desirable, consistent orientation of the satellite without coning; other solutions may exist (7:3). In this attitude, the satellite's spin axis is aligned with the angular momentum vector.

As expected, symbolic linearization using *Mathematica* (28) led to a 5 x 5 Jacobian matrix having a zero row and column for h_2 , representative of a zero eigenvalue. The row and column were removed, resulting in the following fourth order linear system

$$\dot{\mathbf{Z}} = \begin{bmatrix} 0 & -\frac{\varepsilon'}{B} - 1 & \frac{b}{B} & 0 \\ \frac{I_1 - 1}{I_1} & 0 & 0 & \frac{-b\varepsilon}{I_1} \\ -\frac{\varepsilon}{I_1} & -\frac{c}{B} & \frac{cI_3}{\varepsilon B} & -\frac{b\varepsilon^2}{I_1} - k \\ 0 & \frac{1}{B} & -\frac{I_3}{\varepsilon B} & 0 \end{bmatrix} \mathbf{Z} \quad (17)$$

where

$$B = b\varepsilon - \varepsilon'I_3$$

$$\mathbf{Z} = \begin{bmatrix} h_1 \\ h_3 \\ p_n \\ x \end{bmatrix} \quad (18)$$

Equations 17 and 18 are the dynamical relations used in the following analyses.

Stability Criteria

The general stability criterion states that, for a quasi-rigid body with very slow energy dissipation, only spin about the major axis is asymptotically stable. Additional stability criteria must also be included. For this case, in which the nutation damper provides the energy dissipation, the analysis becomes more complicated. Linearization was used to find stability conditions by Sarychev and Sazonov (20:295) while Hughes

used linearization and the Routh-Hurwitz criteria (15:151). Chinnery verified these conditions using a Liapunov function (8:24). Chinnery and Hall defined the stability criteria (7:3) in terms of the dimensionless parameters (Equations 9, 10) as

$$\begin{aligned} I_2 &> I_3 \\ I_2 &> I_1 + \frac{\varepsilon^2 b}{k} \end{aligned} \quad (19)$$

However, we know from the non-dimensional that $I_2 = 1$; therefore, the minimum stable spring constant (7:3) is found

$$k_{crit} = \frac{\varepsilon^2 b}{1 - I_1} \quad (20)$$

With the requirements listed in Equations 19 and 20, the satellite's stability is maintained but the degree of stabilization is the focus of this analysis. The degree of stability can be defined by the location of the eigenvalues in the complex plane (a more stable system has eigenvalues farther into the left-half plane). Correspondingly, the maximum degree of stability coincides with the minimum transient duration of the coning motion (20:295). Thus, further analysis attempts to find the set of parameters which maximizes the stability of the system.

III. Damping Effects

The amount of energy dissipation caused by a nutation damper can easily be altered by varying its characteristics, namely the spring constant, damping coefficient, and particle mass. In this problem, however, the nutation damper is attached to a rigid body, the satellite. This introduces additional parameters which affect the overall, coupled motion of the system. The following chapter discusses the importance of such characteristics as the damper placement, system moments of inertia, and the ratio of particle mass to system mass are discussed. It also reviews a method of eigenvalue analysis used to study damping and relates the method to the peculiarities of this problem. Lastly, this chapter analyzes how each parameter affects damping and the system's overall motion.

Eigenvalue and Eigenvector Analysis

Given four linearized, homogenous equations defined in the previous chapter (Equation 17), we must now attempt to find the system's eigenvalues to determine attainable degrees of stability. Using the eigenvalues to determine the damping characteristics is common in dynamical analysis. This method, in a mathematically uncoupled system, provides two second order problems and a simple method for analyzing the damping of separate components: the rigid body and the spring-mass-damper. The fourth-order system presented here provides distinct, coupled eigenvalues. However, second order analysis principals apply.

In a second order problem, the characteristic roots describe the damping of the simple system. The *damping time index*, as proposed by Borelli and Leliakov (5:345), is defined as the "largest real part of the characteristic roots of the system model, linearized about the equilibrium attitude." It is simply the inverse of the non-dimensional time to damp out the coning motion of the system. For a damped, stable system, all eigenvalues lie in the left-half plane and minimum time damping occurs when the real eigenvalue part is a minimum.

Eigenvalues may consist of a real part, which describes the inverse damping time, and a complex part, equal to the damped frequency. In underdamped second order systems, a complex conjugate eigenvalue pair appears in the complex plane, as seen in Figure 2. Underdamped systems will eventually damp out, but at a much slower rate than desired. Overdamping occurs when real and distinct eigenvalues are present, leading to a lengthy damping time. Lastly, critical damping is the optimal solution to a second order damped system, where two identical, real roots exist. This damping type will induce a zero amplitude relatively quickly as seen below.

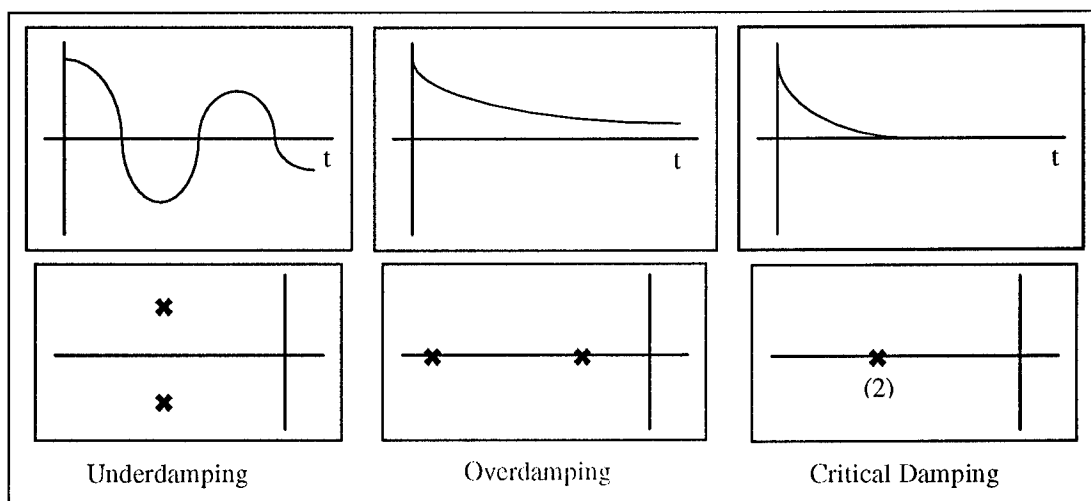


Figure 2, Damping Over Time and Eigenvalues for Damping Types

Since the four-component Y vector is composed of $\{h_1, h_3, p_n, x\}$, the eigenvector can be used to analyze the degree to which each component plays a role in the corresponding eigenvalue and, therefore, the system stability. The angular momenta, h_1 and h_3 , are somewhat representative of the rigid body's motion (denoted RB, above), while the particle's position, x , and momentum, p_n , are descriptive of the spring-mass-damper's motion (denoted SMD, above).

By comparing the magnitudes of the components of the eigenvectors, the degree of coupling can be determined. As can be seen in the eigenvectors above, the magnitude of the fourth component, the mass particle position, x , is dominant. This implies that the system is heavily dependent upon x and that the system is highly coupled between the spring-mass-damper and rigid body. For clarification purposes, the eigenvalues of the system's angular momentum will be referred to henceforth as the rigid body pair while those of the particle mass and momentum will be referred to as the spring-mass-damper pair.

Independent Parameter Effects

The first step in analyzing the effects of the six parameters relating to this problem is to study their independent effects. Table 1 reviews the parameters which make up the linearized equations of motion (Equations 17, 18).

Table 1, List of System Parameters

c	damping coefficient
k	spring constant
b	distance to damper
I_1	moment of inertia about e_1
I_3	moment of inertia about e_3
ϵ	mass fraction

Recall that $\epsilon' = 1 - \epsilon$. All of the parameters above are included in this optimization study.

Results generally show that one pair of the eigenvalues can be effectively modified by changing a system parameter, while the other pair remains relatively constant. Figure 3 characterizes the movement of the eigenvalues over a range of parameters. This figure shows that one pair of eigenvalues, in this case the one relating to the spring-mass-damper, becomes real, and thus critical damping is possible. Unfortunately, the other pair of eigenvalues, representing the rigid body, varies little over a range of parameters and will never allow truly critical damping.

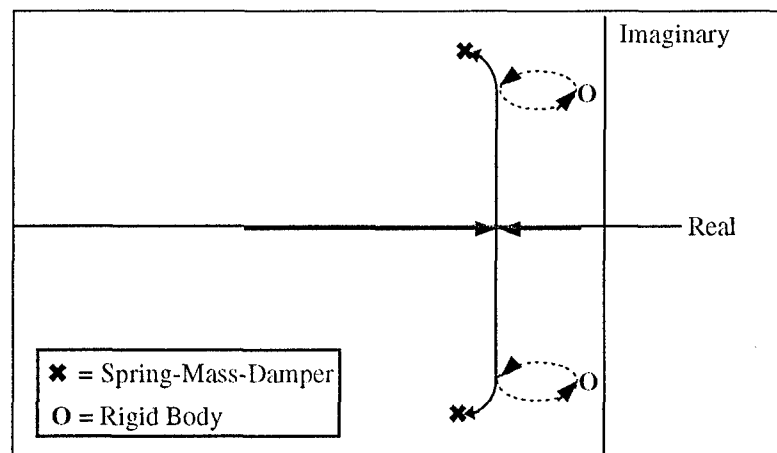


Figure 3, General Variation of Eigenvalues

Since the rigid body's eigenvalues never become completely real, critical damping of either component by tuning the imaginary parts of the eigenvectors to zero, is not a desirable solution to this problem. In a simple, uncoupled spring-mass-damper, the critical damping factor is found by equating the imaginary eigenvalue part (the frequency) to zero. This relation reduces to

$$c_{crit} = 2\sqrt{k\epsilon} \quad (22)$$

While this value drives the particle mass toward equilibrium quickly, it causes the damper's effect on the rigid body to be negligible. Because of the system's coupling, it is not desirable to concentrate analysis upon either individual component, but to study the rigid body and spring-mass-damper stability simultaneously.

Note, in the figure above, that at the point where the rigid body eigenvalues are a minimum, the two pairs' paths cross. Analysis of specific values shows that the eigenvalues themselves truly do approach equality at optimum, not just their paths. This implies that simply equating the rigid body and spring-mass-damper's frequencies optimizes the damping. This technique is one used in classical tuning practices, however it assumes a physically uncoupled model in which the spring-mass-damper has no effect upon the rigid body.

Analysis of the parameter effects of this system begins with a discussion of the changes in the eigenvalues over each parameter, while other parameters are held constant. Next, hypotheses on their coupled effects are made and studied. Figures 4-8 depict a general set of eigenvalues over a range of the given parameter. The plots below are not to scale and are only meant to be representative of the effect of the parameter on the eigenvalues.

From Figure 4, below, it can be seen that the real part of each rigid body eigenvalue is decreased in the complex plane while maintaining a near-constant complex part (frequency). It is evident from this effect that increasing the distance from the rigid body's center to the spring-mass-damper, b , promotes a faster damping rate. An improved response occurs since, for the torque-free assumptions of the second chapter,

the spring-mass-damper applies the sole force which, when coupled with a distance, b , creates the restoring torque. Based upon these findings, the damper placement is considered an independent parameter which has a noticeable effect on the damping of coning motions.

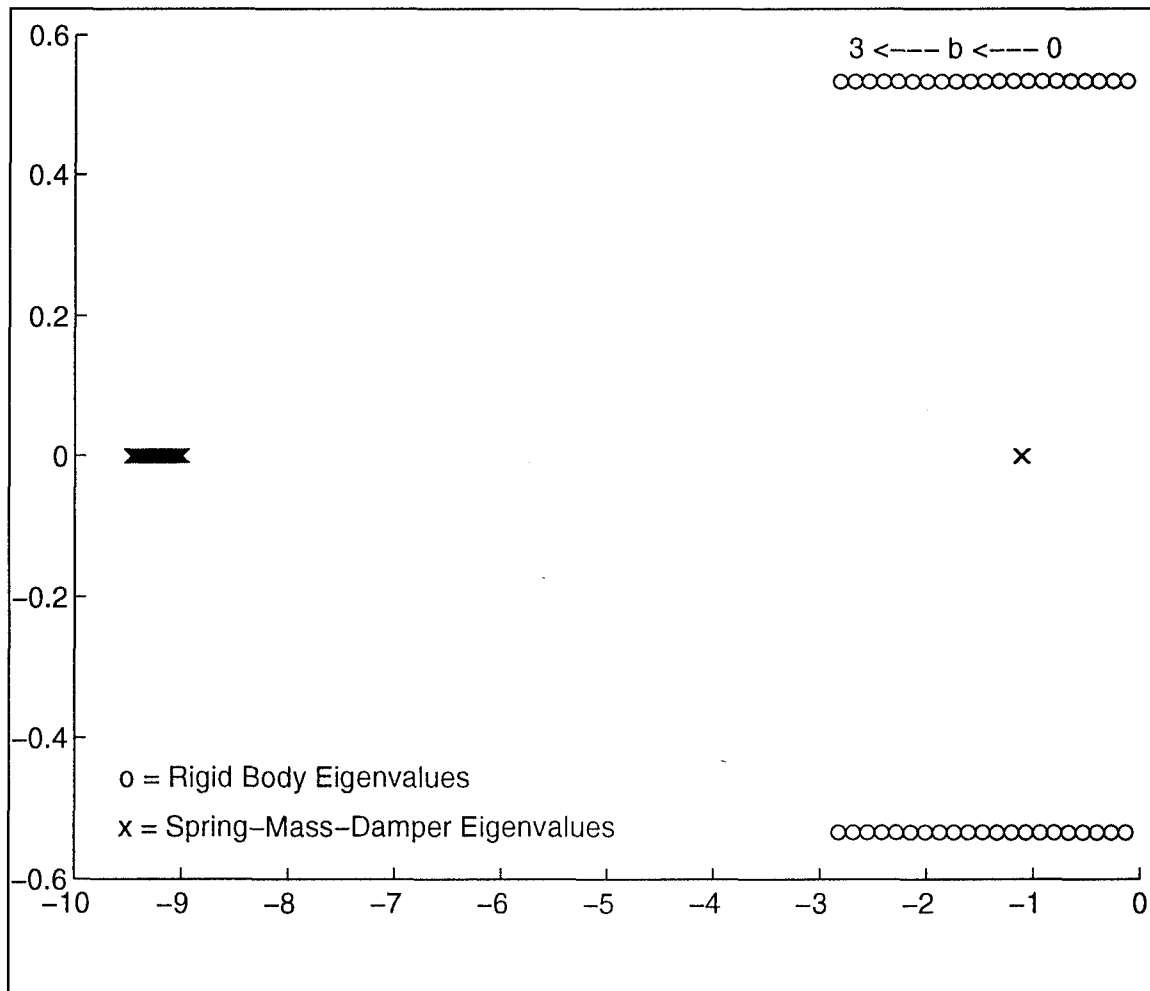


Figure 4, Effects of the Spring-Mass-Damper Placement, b

Figure 5, below, helps to describe the effect of the damping coefficient on the system's eigenvalues. The eigenvalues resulting from an increased damping coefficient decrease to a minimum. This minimum occurs for a relatively small damping coefficient, as the spring-mass-damper's frequency approaches that of the rigid body. Again, this

implies that tuning the rigid body and the spring-mass-damper's frequencies optimizes the system.

Note that at some critical value for c , the spring-mass-damper's eigenvalues approach, then become real. It is at this point that the spring-mass-damper, by itself, becomes critically damped, while the rigid body does not.

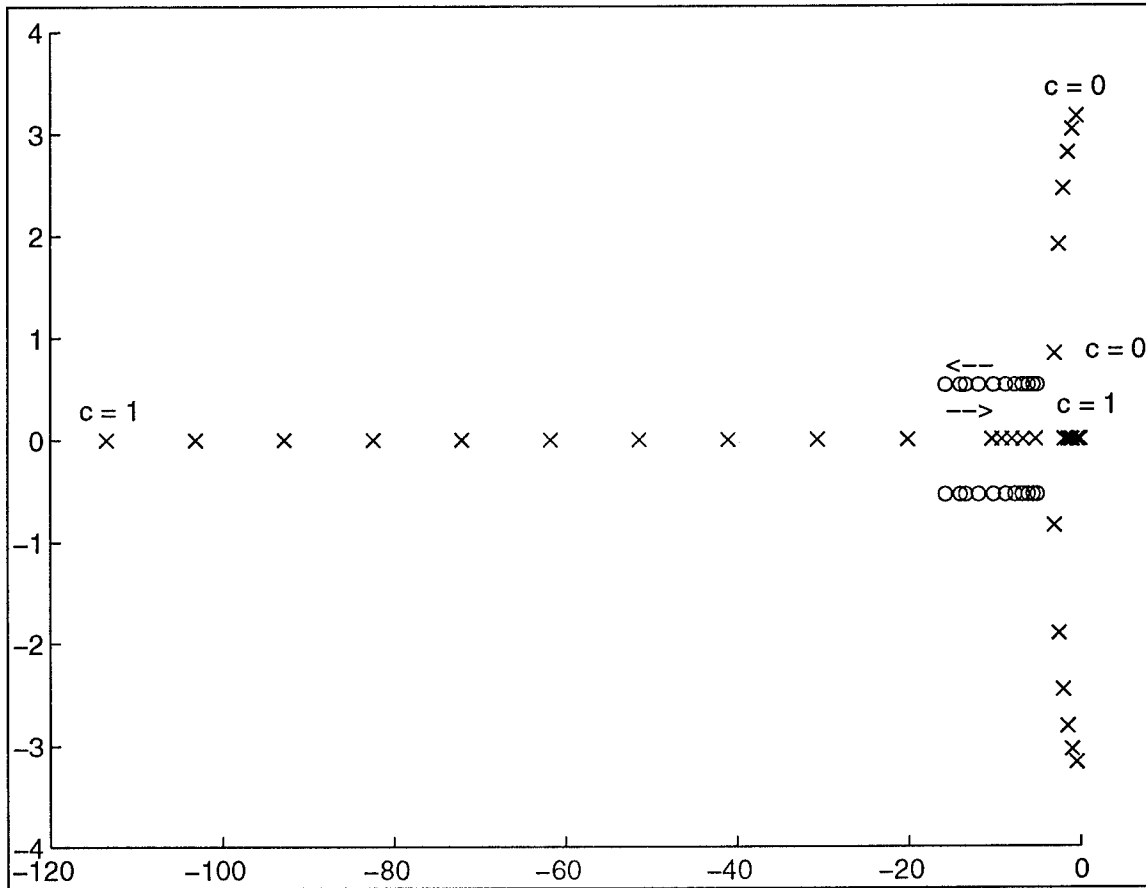


Figure 5, Effects of the Damping Coefficient, c

As discussed in the stability section of Chapter 2, the system will be unstable for very small values of k , the spring constant. Figure 6 includes the region where $k < k_{crit}$ and shows that, for very small k , the spring-mass-damper's eigenvalues begin in an unstable region (to the right of the dashed line), become overdamped (two distinct, real

eigenvalues), critically damped (two identical, real eigenvalues), then underdamped (a complex conjugate pair). Underdamping occurs as a result of a constant, small c , and a relatively large k for a given set of parameters. Thus, it appears that the damping coefficient may have to increase somewhat for increasing spring constant. The degree of proportionality between c and k for optimal solutions will be discussed in Chapter 4.

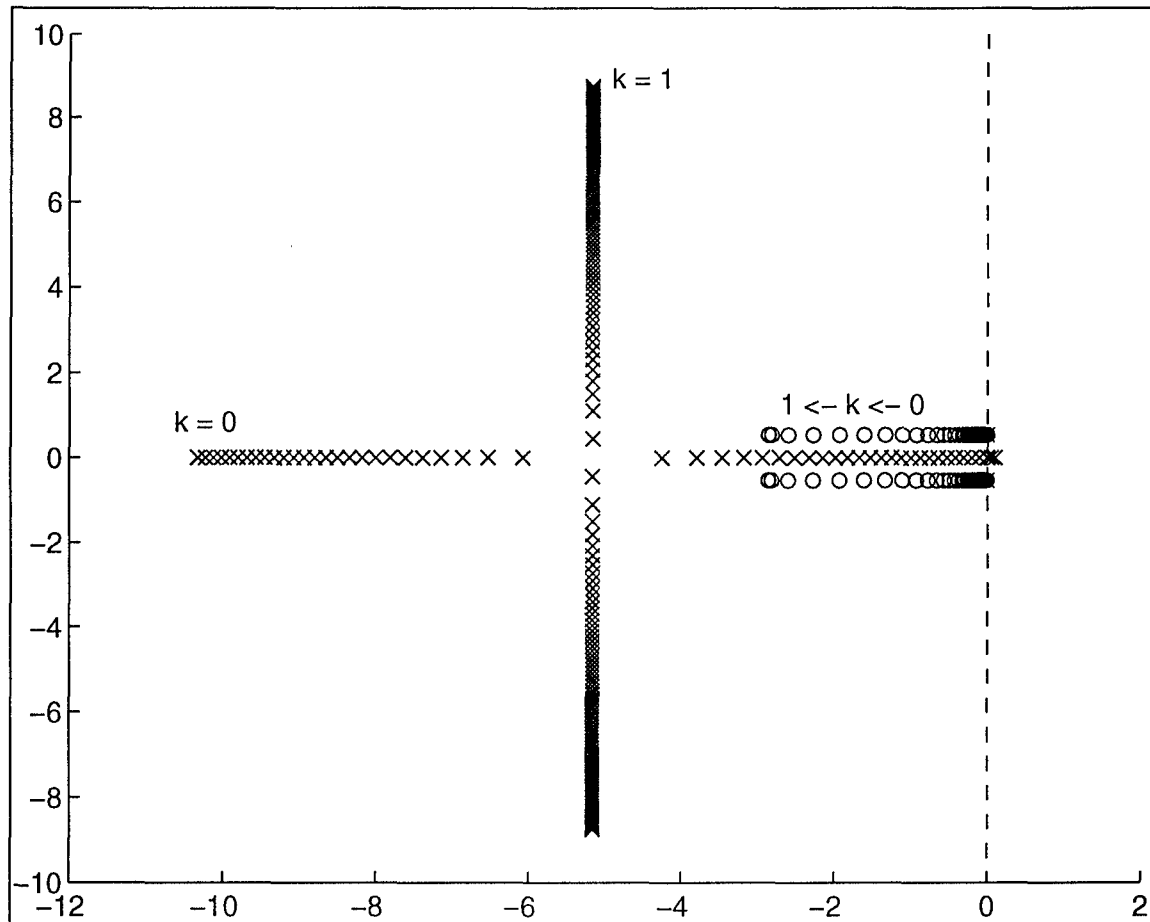


Figure 6, Effects of the Spring Constant, k

Figure 7 shows the trend of the rigid body eigenvalues to become more negative as the moments of inertia increase in proportion to each other. This implies that an asymmetric body is more stable than an axisymmetric one. However, as I_1 increases, the real eigenvalue parts far exceed those produced when I_3 increases. Recall that I_1 is the

moment of inertia about the direction of the spring-mass-damper as shown in the System Model (Figure 1).

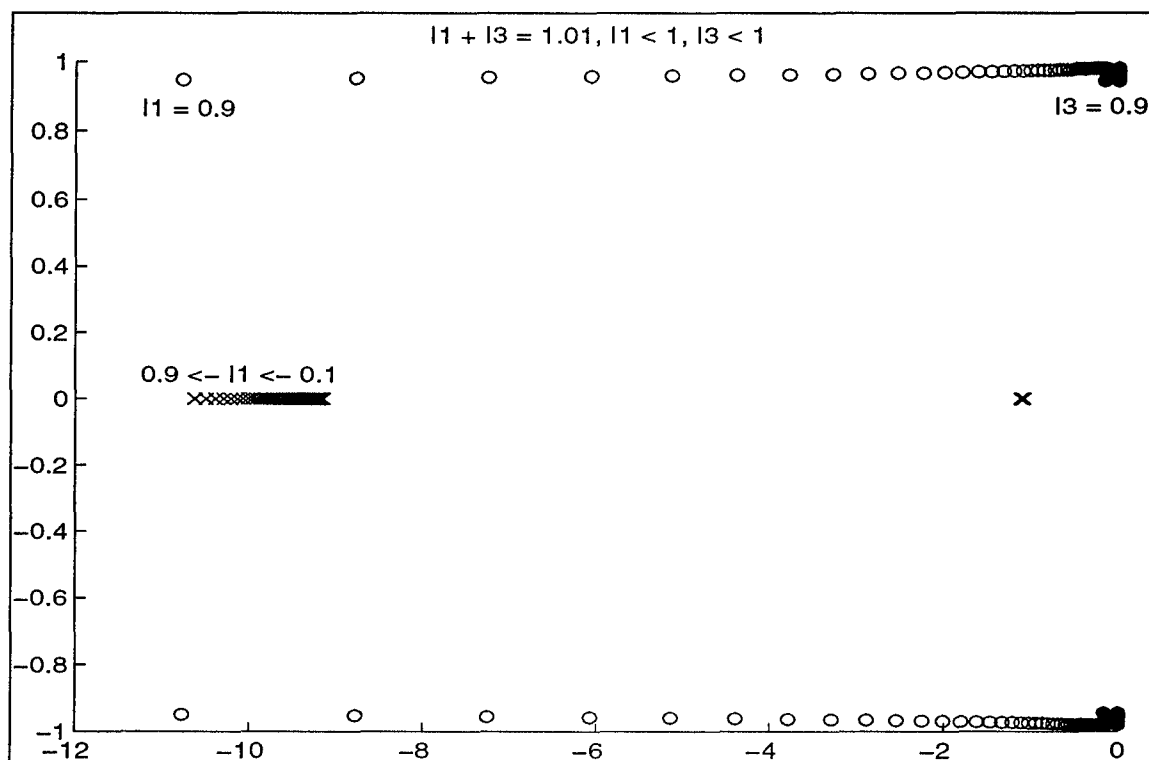


Figure 7, Effects of the Moments of Inertia, I_1 and I_3

With a relatively small moment of inertia about the e_3 axis, the effect of the spring-mass-damper is greater because of a lesser moment to overcome. Since typical satellites are fairly symmetric, further analyses use values of I_1 and I_3 which are similar.

The results of the effects of the moments of inertia could be used by satellite designers to select satellite component placements which are along the e_3 direction, giving rise to a smaller relative I_3 . Allowing asymmetry affords a much larger array of alternatives for the designer, however for large initial coning angles the nutation damper may not always be the most efficient (21:222).

Figure 8 describes the effect of the mass fraction upon the eigenvalues of the system. As the mass fraction increases, the rigid body eigenvalue decreases, thus improving the damper's effect. Meanwhile, the spring-mass-damper eigenvalues converge to a point, then become complex, indicating underdamping. As expected, for constant damper placement, damping coefficient, spring constant, and moments of inertia, it is more desirable to have a large mass fraction. This result supports the notion that a greater particle mass will have a greater effect on the coning motion, while the stability criteria of Equation 20 is maintained.

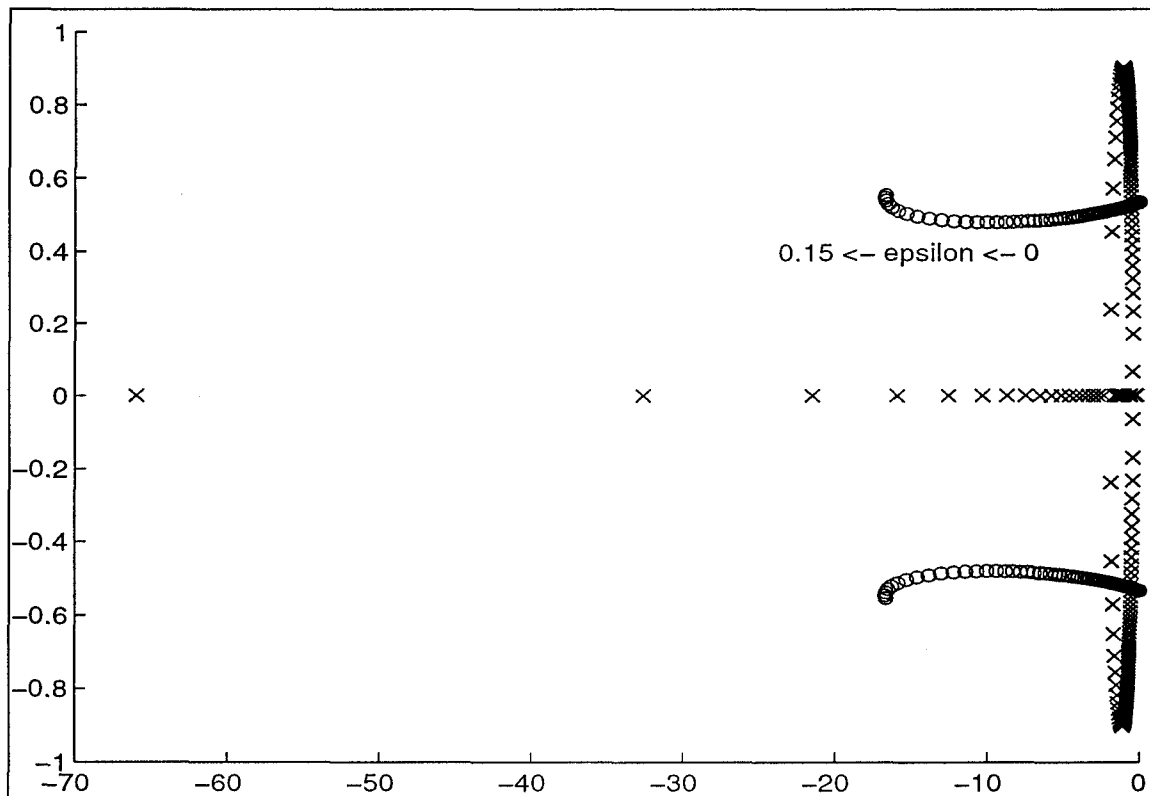


Figure 8, Effects of the Mass Fraction, ϵ

IV. Optimization Problem

As discussed in Chapter 3, it is apparent that the eigenvalues representative of the rigid body will never become real so no truly critical damping exists. Thus, an optimization problem arises in which the time until the system damps out is minimized. The optimization is accomplished by maximizing the magnitude of the real part of the rigid body eigenvalue. This chapter sets up the optimization problem, describes methods of solution, and provides basic optimization results.

Maximization of the Damping Rate

The non-dimensional damping rate is simply the real part of the eigenvalue in question. This is true because, as in the general second order case, the complex part of the eigenvalue equals the damped frequency while the real part is the damping rate. The general expression is

$$F(t) = e^{\sigma t} (A \cos \omega t + B \sin \omega t) \quad (23)$$

where the eigenvalue is equivalently

$$\sigma + \omega i \quad (24)$$

In Equation 23, the damping rate is clearly maximized as $|\sigma| \rightarrow \infty$ for an exponentially decaying function. This result implies that the magnitude of the real eigenvalue part must be maximized in order to intensify the damping rate of coning motions. Recall that, for stable solutions, eigenvalues lie in the left-half plane, ensuring that $\sigma < 0$.

Using the second order damping characterizations of the previous chapter (Figure 2), the solution to this fourth order problem lies in a study of its eigenvalues. While the two pairs of eigenvalues are not truly uncoupled, they are characterized by the components of the state vector which they represent. Recall that the rigid body eigenvalue pair is referred to as the ones which represent the eigenvectors for the angular momentum components and the spring-mass-damper eigenvalues as the ones which represent the mass particle position and linear momentum.

At this point, all of the parameters necessary to set up an actual optimization problem have been introduced and the model has been shown to be highly coupled (Chapter 3). The problem is reduced to finding the minimum real part of the rigid body eigenvalues from the Jacobian matrix (Equation 17), given the stability criteria as described in Chapter 2 (Equations 19-21). The system parameters are b , c , k , I_1 , I_3 , and ϵ ; however the analysis of Chapter 3 has shown that only c and k have noticeably dependent effects on an optimal solution.

Minimization Methods

Unfortunately, symbolic eigenvalues are unattainable using *Mathematica* (28) software. If the symbolic eigenvalues could be found, equating the partial derivatives of the real part of the rigid body eigenvalue with zero would lead to an analytical minima. Results lead to lengthy, unusable equations and numerical optimization is necessary.

MatLab (27) has functions *fmin* and *fmins*, which lead to efficient, numerical results. The function *fmin* is used to find the minimum of a function of one variable, using

adjustable tolerances and ranges. The *fmins* function is very similar, finding the minimum of a multivariate function using unconstrained nonlinear optimization. In this function, the Nelder-Meade simplex algorithm uses the direct search method to compute minima. The *Matlab* manual provides additional information (18:77-80). As an example, the *fmins* function could be used to find a set $\{c, k\}$ yielding the minimum real eigenvalue parts of the rigid body pair, given the rigid body characteristics $\{b, \varepsilon, I_1, I_3\}$.

Effects of Varying the Damping Coefficient

Based upon the independent effect analysis of Chapter 3, the damping coefficient which yields a minimum real eigenvalue is relatively small. In addition, the magnitudes of the damping coefficient and spring constant are somewhat proportional. This section verifies these hypotheses and discusses their implications through illustrations.

Prior analysis using the method of multiple scales has postulated that the real eigenvalue parts are a concave function of the damping coefficient (6:165). Using the exact, linearized model relationships (Equations 17, 18), numerical results support this effect. As seen in Figure 9 on the following page, a very small damping coefficient results in real eigenvalue parts of much greater magnitude. To make this plot, constant values of $b, I_1, I_3,$ and ε are used, minimizing the real eigenvalue parts while varying k . Note that for a larger damping coefficient, no improvements in the damping rate are attained. Further focus shifts to lightly damped regions, where values of c are small.

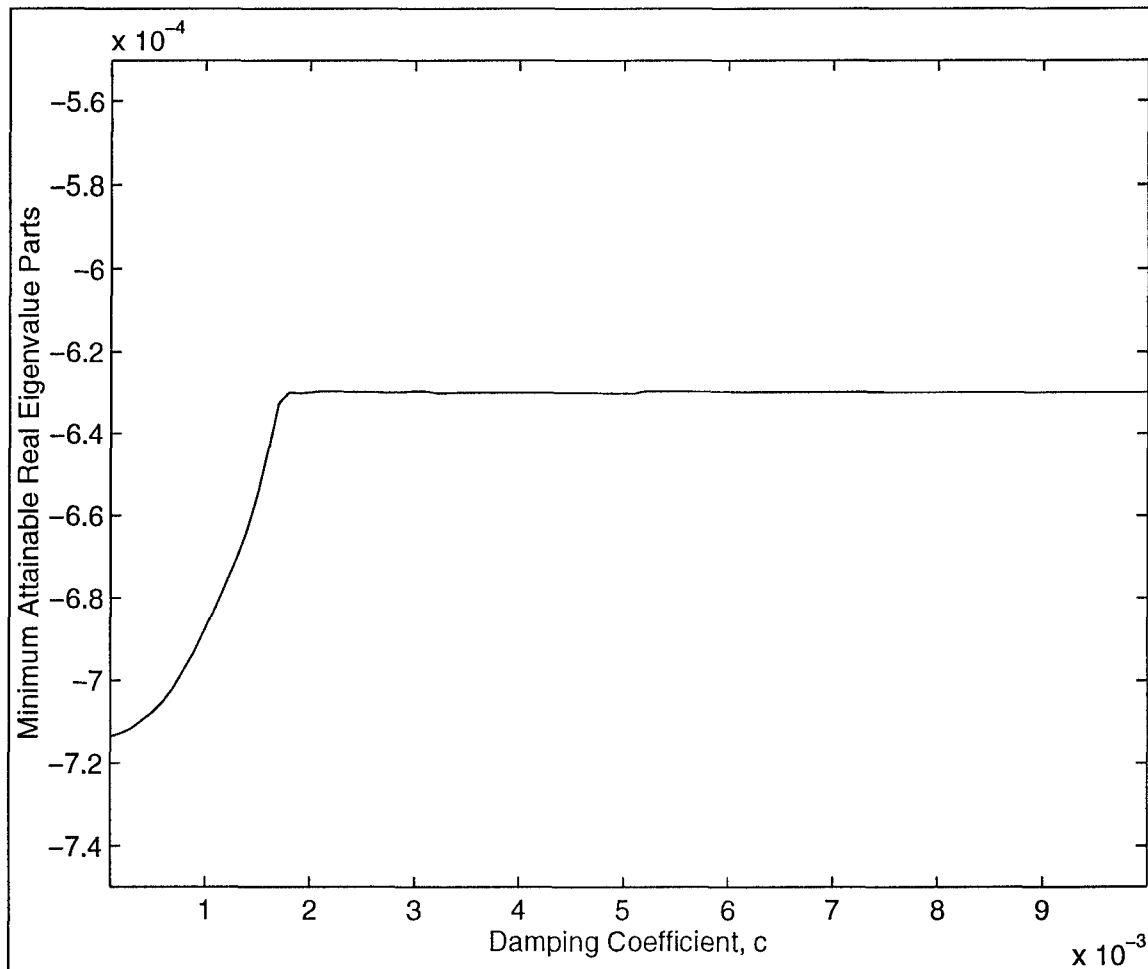


Figure 9, Real Eigenvalue Part Dependence Upon the Damping Coefficient, c

Based on this analysis, the system must be lightly damped in order to achieve improved damper response. Should designers impose “off-the-shelf” parts or limit the damping coefficient in any way, sub-optimal results are expected and the spring constant selection becomes even more important. A better understanding of the relationship between c , k , and their combined effects on the eigenvalues requires a study of the effects of varying the spring constant.

Effects of Varying the Spring Constant

Recalling the minimum spring constant defined by Equation 20 (of the order of 10^{-4}) and considering Figure 10, it is apparent that only relatively small values of k will result in a minimum damping time. Note that the minimum of the real part of the spring-mass-damper's eigenvalue occurs at a slightly larger value than this critical k (for the values used here, $k_{crit} = 0.00025$).

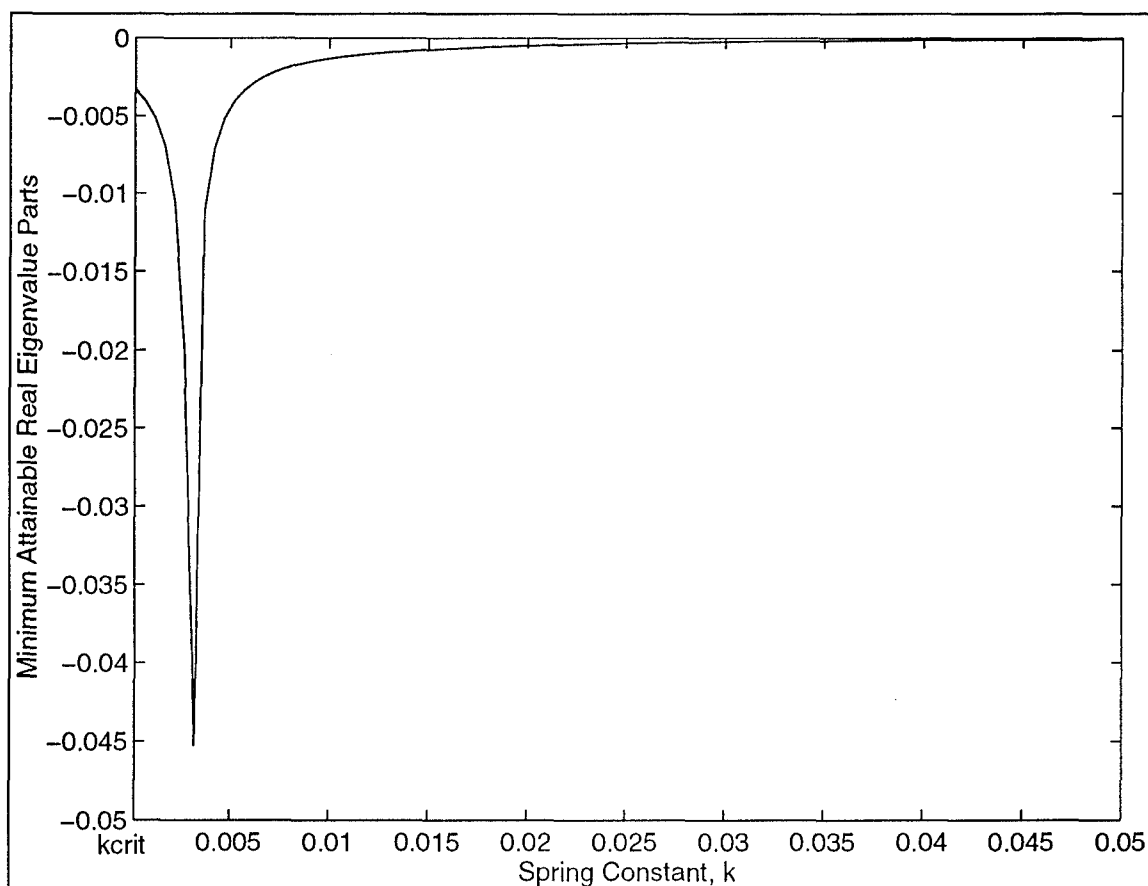


Figure 10, Real Eigenvalue Parts Effects Based Upon the Spring Constant, k

In the figure above, the minimum real eigenvalue approaches zero as the spring constant exceeds 0.005. Recall that, in Figure 9, the damping coefficient was also

relatively ineffective as it exceeded the same order of magnitude. This implies that the two are somewhat proportional, at least in regions beyond the optimal solution. Figure 11, confirms that the damping coefficient and spring constant are almost linearly related for regions beyond optimal, and that a minimum damping coefficient is achieved at the optimal solution.

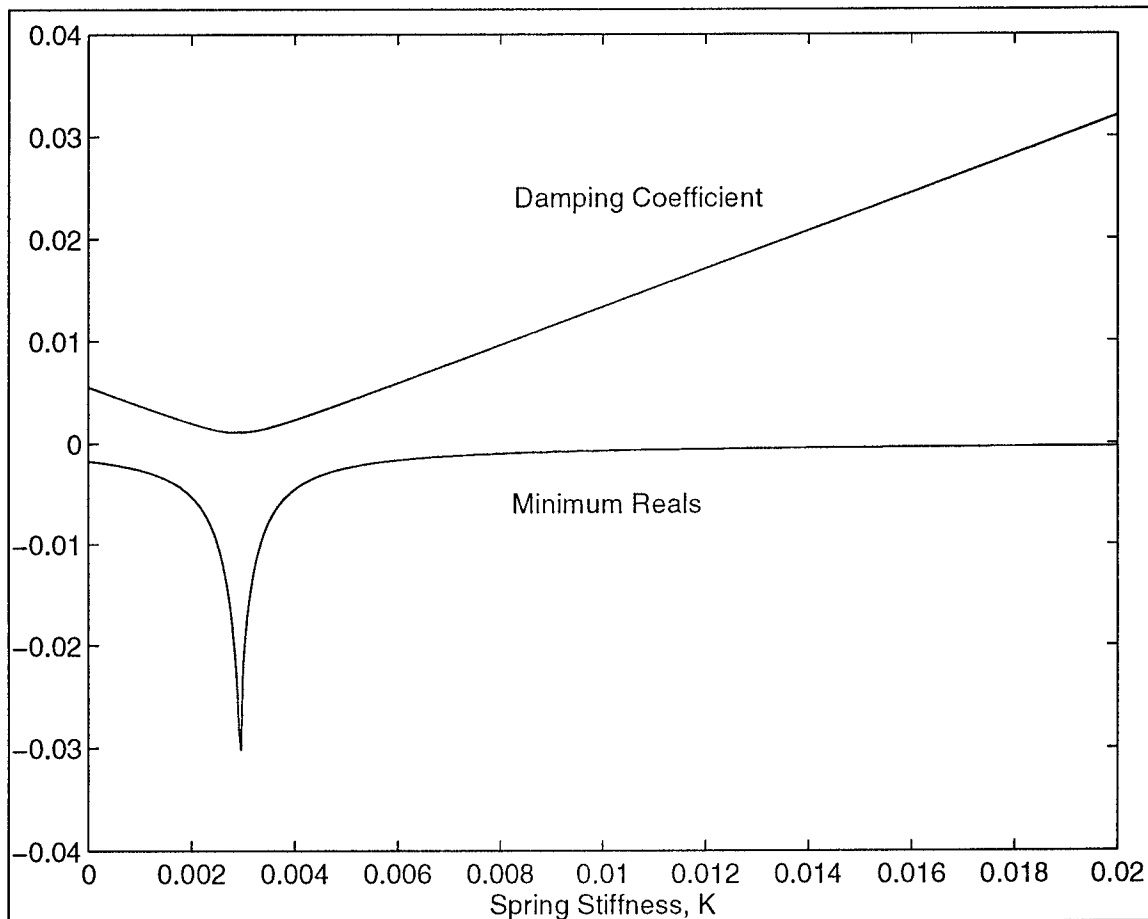


Figure 11, Damping Coefficient and Spring Constant Relation for Minimum Reals

Effects of Varying the Location of the Spring-Mass-Damper

The placement of the spring-mass-damper in relation to the center of mass of the rigid body has a significant effect upon the real part of the system's eigenvalues, a key to

determining the time required to damp out coning motions. While the analysis of Chapter 3 held the spring constant and damping coefficient constant, the optimized effects of the damper location are now illustrated.

The non-dimensional distance from the rigid body's center of mass to the equilibrium point of the spring-mass-damper, b , plays an even greater role when minimizing the real eigenvalue parts as functions of c and k , as seen in Figure 12. Numerical analysis shows that as b increases, the eigenvalues' real parts decrease, thus increasing the damping rate of the coning motion. Very small values of the eigenvalues' real part are attainable by extending the distance to the spring-mass-damper. This occurs as a result of the torque caused by the nutation damper and its proportional increase with distance.

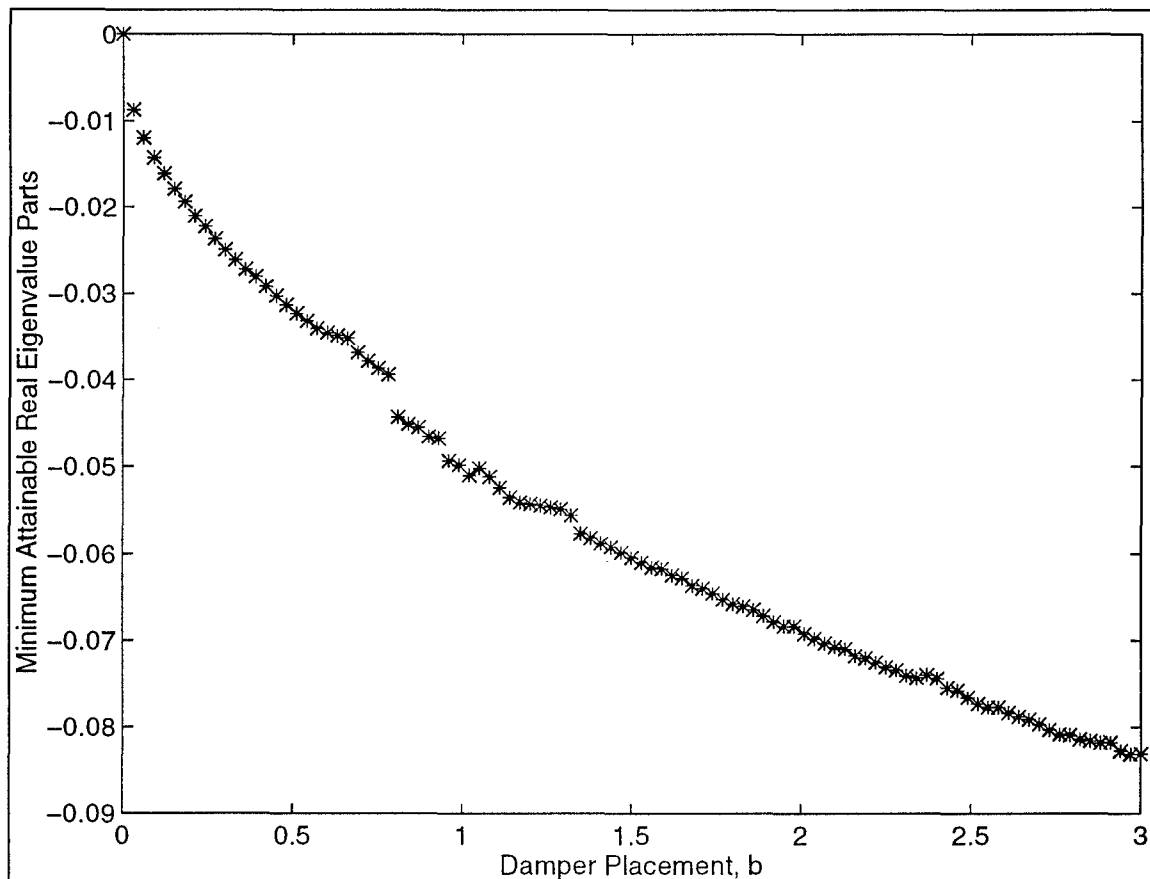


Figure 12, Minimum Real Eigenvalues for a Practical Range of b

As seen in Figure 13, the magnitude of the real part of the eigenvalues not only becomes relatively large as b is increased, but a distinct minimum occurs for specific values of the spring constant. Numerical minimization below uses a given value for b over a range of k , then solves for the damping coefficients which yield the minimum real eigenvalue part. These results verify that the minimum real eigenvalues attainable for typical satellite configurations ($b < 1$) lie within the same spring constant region. As the distance to the damper increases, the corresponding optimum values of k tend to increase as well. The large effect of extending the position of the spring-mass-damper could be capitalized upon by designers through the placement of dampers at the end of extendable booms or antennas.

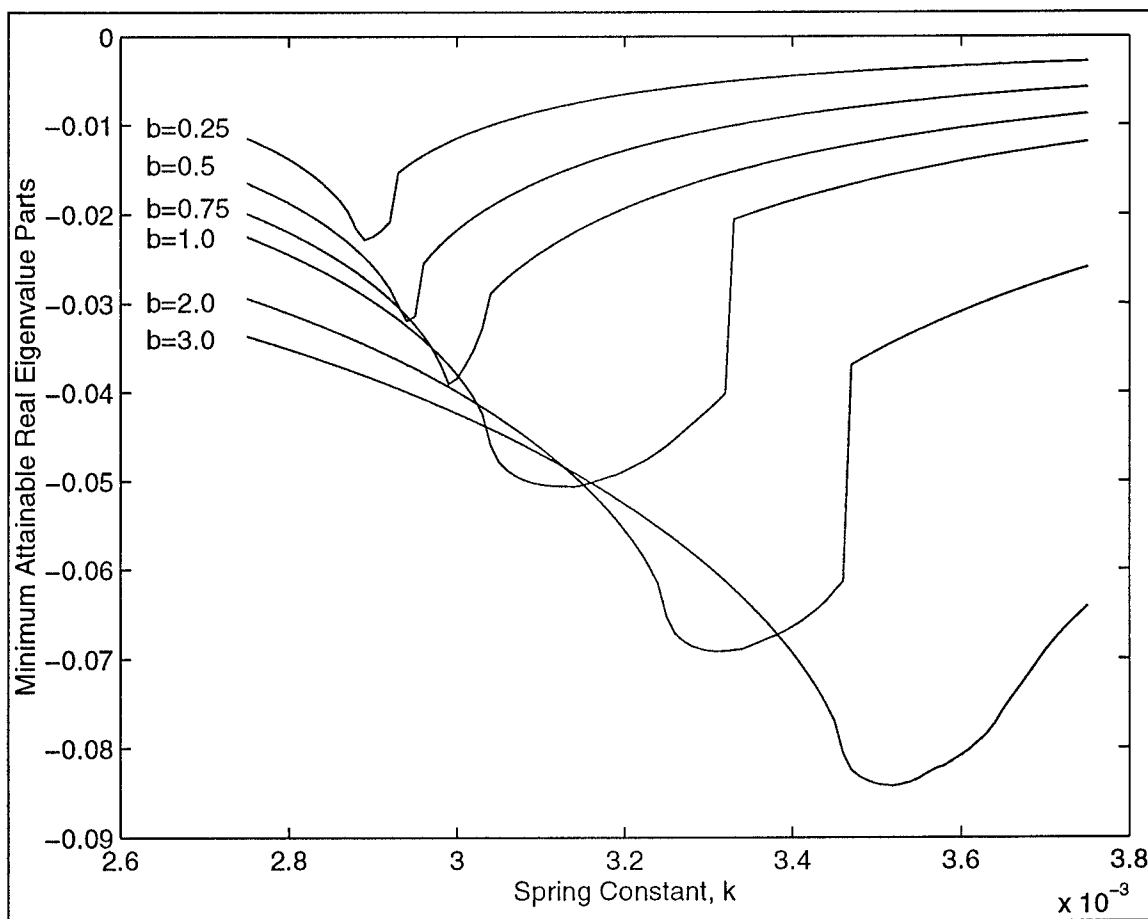


Figure 13, Minimum Real Eigenvalues for $b = \{0.25, 0.50, 0.75, 1, 2, 3\}$

This chapter shows that an optimized solution is obtainable which maximizes the damping rate of the system. Results show that a relatively small c and k are desirable and can provide a distinct minimum to the real eigenvalue parts of the rigid body mode. It has also been verified that faster damping rates are obtainable as the damper's location is extended.

V. Comparisons to a Classical Tuning Method

This chapter compares the optimal solution for the linearized equations of motion to a classical tuning method. This method assumes a completely uncoupled system for the rigid body and spring-mass-damper, incorporating a mathematical analysis to select parameters (6:165, 11:52, 20:298, 21:219). Analysis verifies that this practice is capable of producing favorable damping results, but is inferior to the optimization scheme presented here.

Classical Nutation Damper Design

Historically, dynamicists have designed a nutation damper through a method called “tuning”. Nutation damper tuning equates the rigid body natural frequency to that of the physically decoupled spring-mass-damper. The natural frequency of the rigid body, ω_n , is purely a function of the system’s moments of inertia and is found using Euler’s equations to be

$$\omega_n = \sqrt{\frac{(I_2 - I_1)(I_2 - I_3)}{I_1 I_3}} \quad (25)$$

Next, the non-dimensional damped frequency, ω_d , is found for the decoupled spring-mass-damper

$$\omega_d = \sqrt{\frac{k}{\varepsilon} - \left(\frac{c}{2\varepsilon}\right)^2} \quad (26)$$

After equating them, it is a fairly simple calculation to determine a set of spring constants and damping coefficients which satisfy the tuning condition using the relation

$$c = 2\varepsilon \sqrt{\frac{k}{\varepsilon} - \omega_n^2} \quad (27)$$

In Figure 14, it appears that the eigenvalues of the rigid body and spring-mass-damper approach equality at the optimal solution. This finding supports tuning the frequencies of the decoupled rigid body and spring-mass-damper. The dashed line below is equivalent to the uncoupled rigid body natural frequency found by Equation 25. For this analysis, however, that assumption will not be made and it will be shown that much better results are possible.

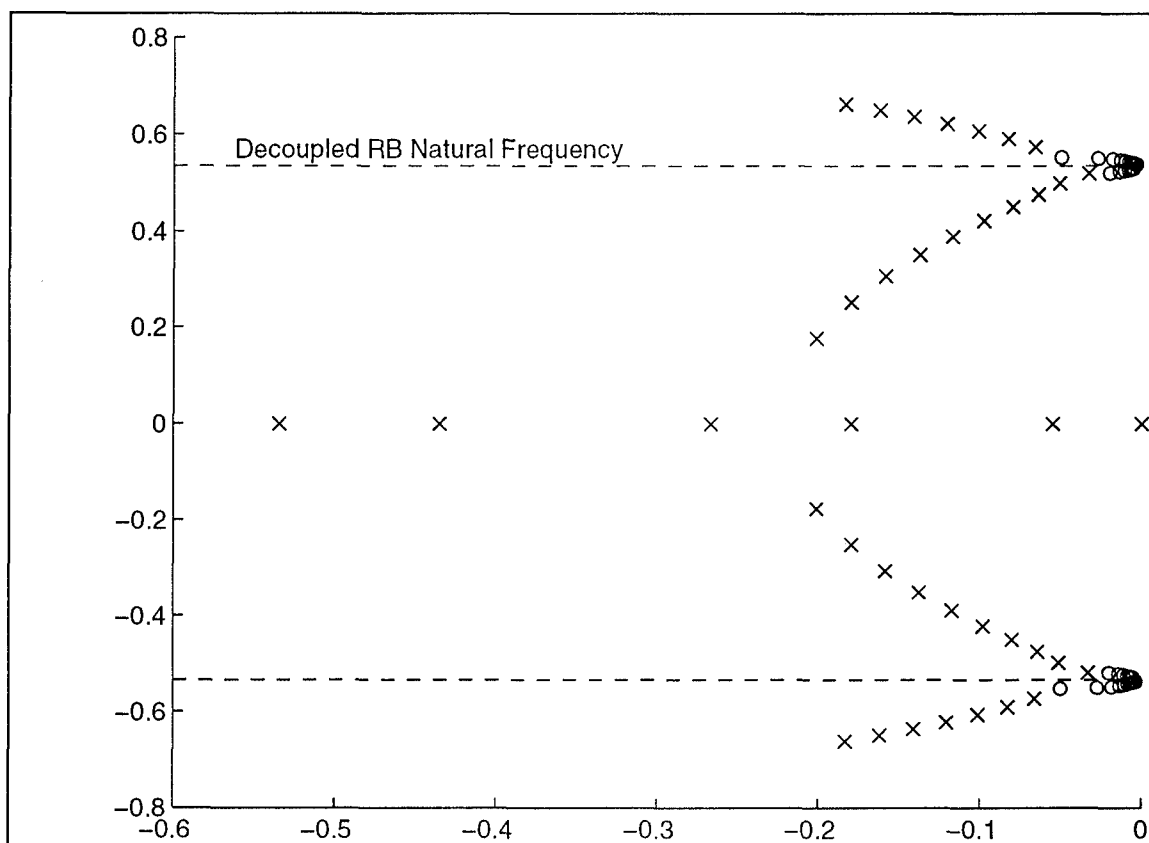


Figure 14, Apparent Eigenvalue Equality at Optimum

Actual Results

Using the physically decoupled tuning method relationship for k and c listed above, damping responses of the numerical optimization and classical tuning are compared. Figure 15 plots the relationship between the damping coefficient and spring constant for optimal methods, as in Figure 11, and classical tuning. The two methods result in different relations for c and k , while both yield similar results at the optimized solution (when c is a minimum). Unfortunately, exact values of the parameters are not available at this point using the decoupled method alone, leading the designer to suboptimal results.

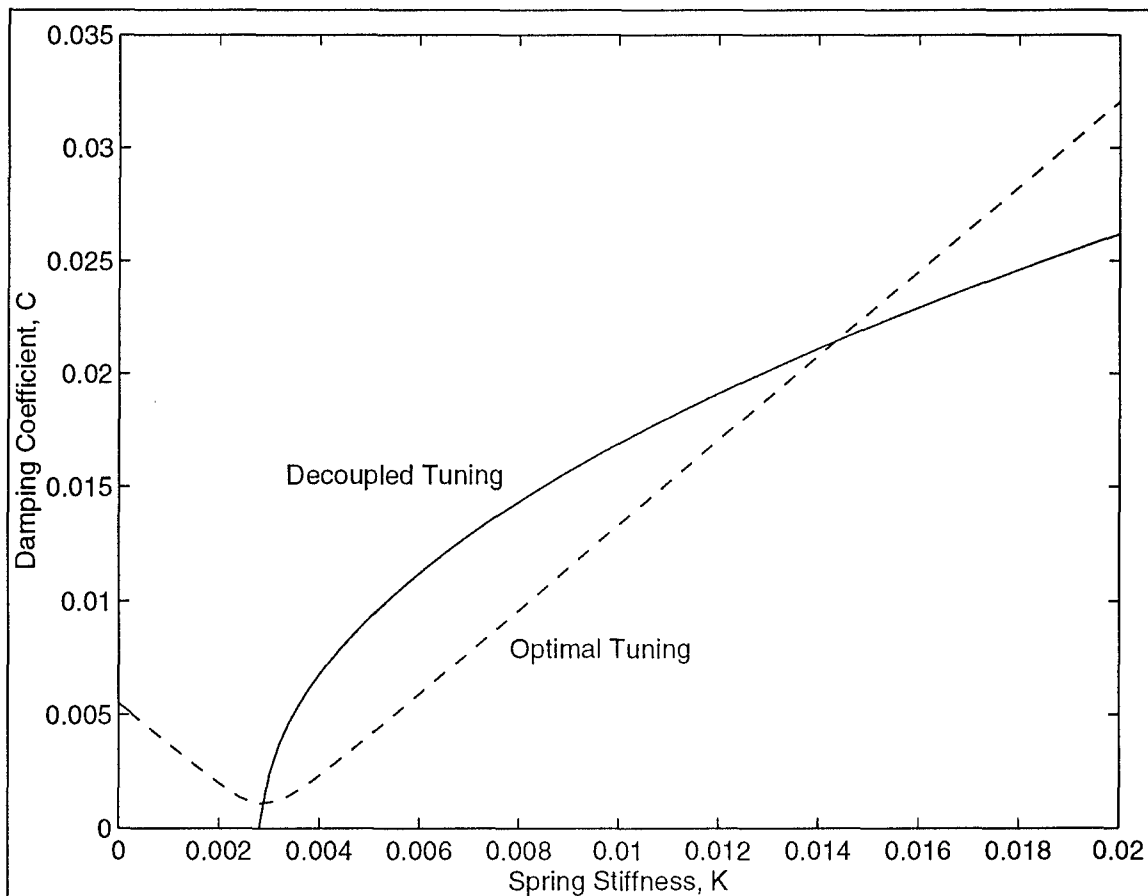


Figure 15, Spring Constant/Damping Coefficient Relationships

A major shortcoming of the decoupled method lies in solutions when the resulting damping coefficient is imaginary. This occurs when the radical term in Equation 27 is negative, when

$$\frac{k}{\varepsilon} < \omega_n^2 \quad (28)$$

This region includes unstable values of the spring constant but also a noteworthy region of viable values for k . For spring constant values outside of this region, no real value for c is obtainable when using the decoupled tuning approach.

Finally, a direct comparison between the two tuning methods is made. Figure 16 shows that classical tuning results in a minimum of real eigenvalues, however limited by Equation 28. In the plot below, a value of $b = 1.0$ is used to illustrate the trend in the differences. The tuned curve uses values of c which are provided through optimization results in order to emphasize the improved performance of optimal methods. In practical applications, designers must arbitrarily select a value for one parameter (c or k), then solve for the other using Equation 27.

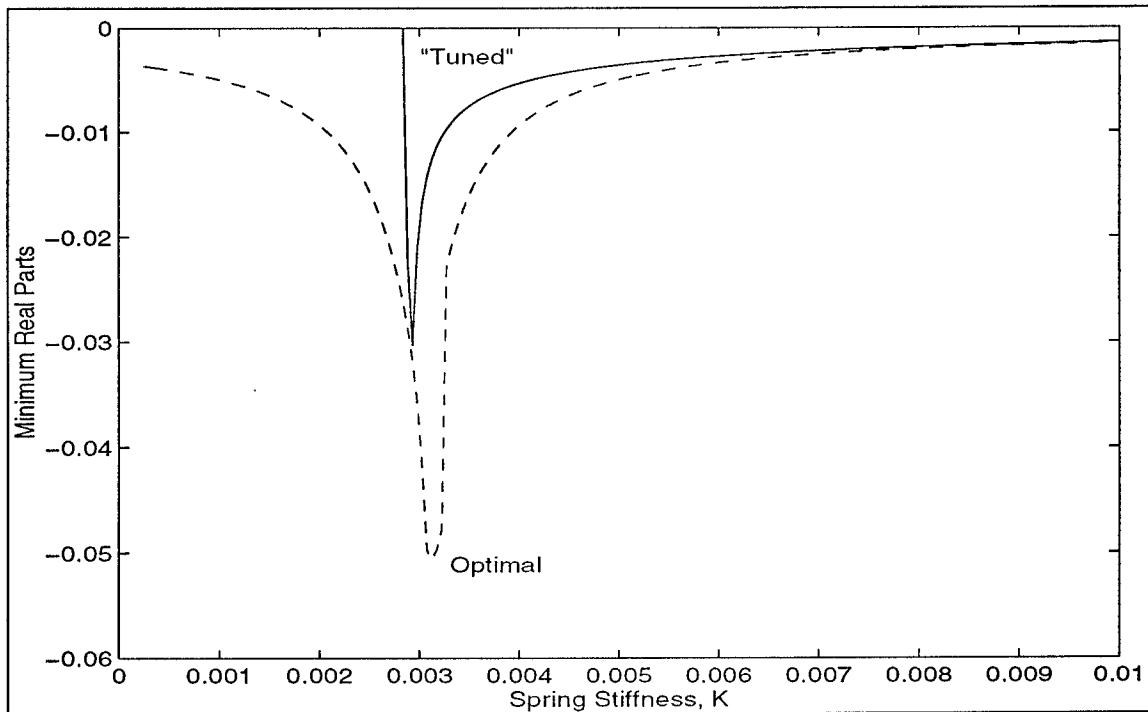


Figure 16, Comparison of Minimum Attainable Eigenvalues

The minimum point on the decoupled tuning curve above occurs when c is slightly greater than zero (Figures 15 and 16). This implies that designers should select the minimum damping coefficient available. While this may seem plausible, available hardware design may limit its practicality. By using optimal tuning, a relationship between the damping coefficient and spring constant is available which offers exact values for c and k .

The differences in the real eigenvalue parts are the key to the realizing the benefits of optimal parameter selection. Figure 17 plots the net gain in damping rates over the same range of the spring constant as seen in Figure 16. The net gain is characterized by

$$NetGain = \|\sigma_{Min}\|_{Optimal} - \|\sigma_{Min}\|_{Tuned} \quad (29)$$

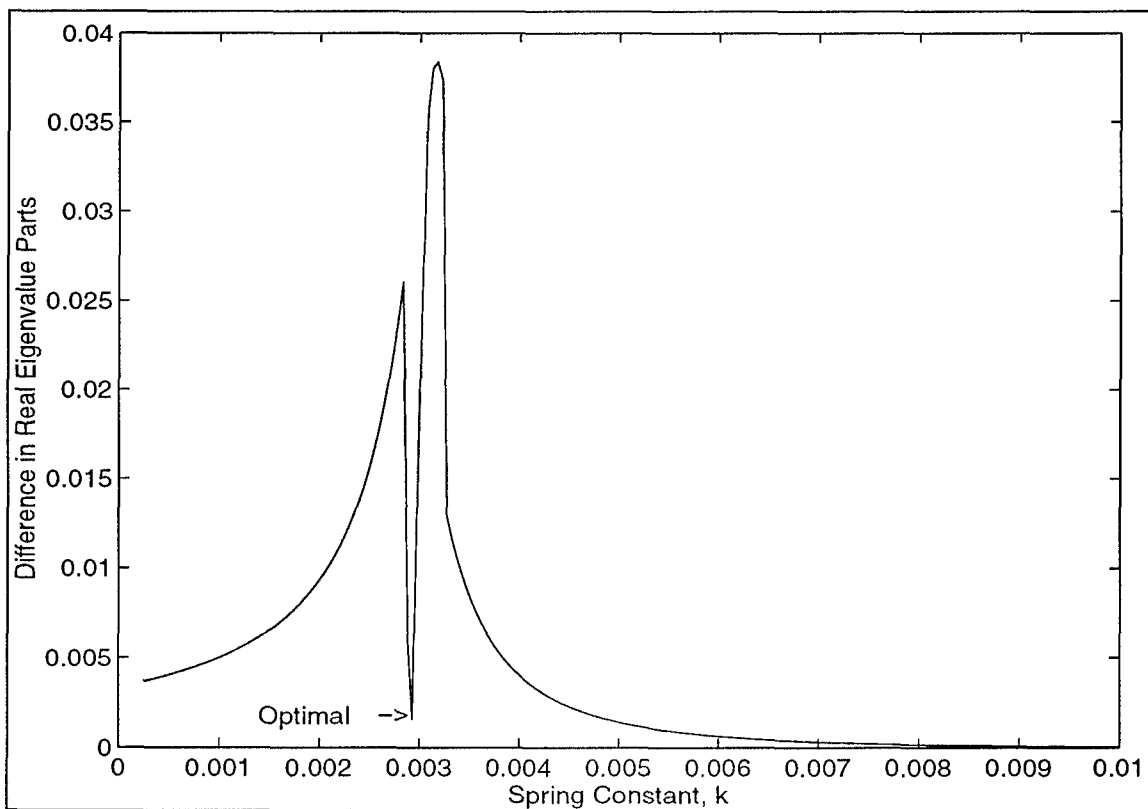


Figure 17, Increased Damping Rates for Optimal Parameter Selection

Here, the function is optimized around the damping coefficient while varying the spring constant. The primary benefit offered by optimal methods is an increase in the optimum region. By inspection of the classical tuning results (Figures 16 and 17), a small change in k has a sharp effect on the magnitude of the damping rate because of the slope of the curve near the minima. Using optimal methods, this effect is reduced by providing a larger region of improved damping rate performance.

In addition to the benefits obtained by optimal tuning methods for a constant damper placement, even greater effects are achieved with increasing b . For the same range of values for b as discussed previously, Figure 18 shows a clear distinction between the damping rates obtained using optimization. Since an exact solution to c is not practically obtainable using classical methods, a constant small c is used ($c = 0.001$). As seen, this seriously limits the performance of the damper when b is less than one.

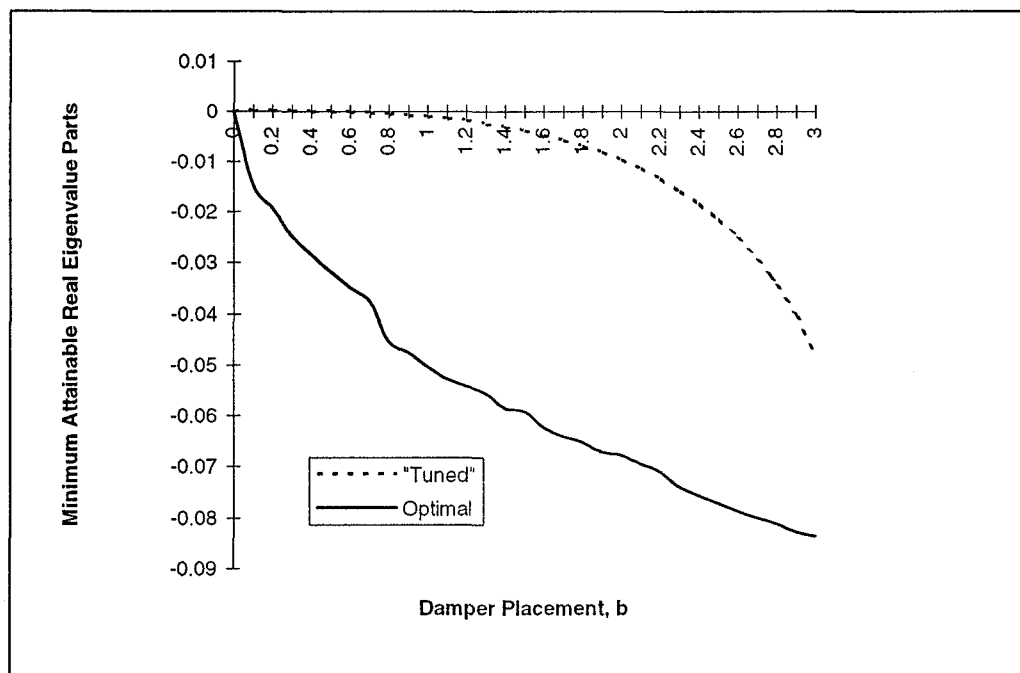


Figure 18, Response of Real Eigenvalue Parts for Tuning Methods

Figure 19 provides a comparison of damping coefficients and spring constants for the same range of b . Note that the uncoupled method does not allow c and k to vary as b is increased.

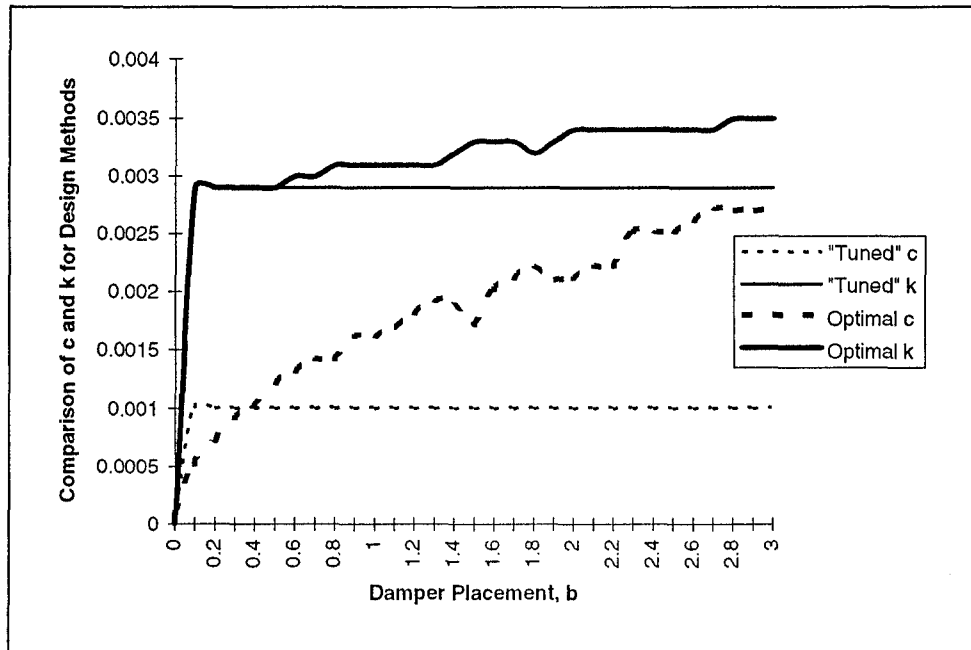


Figure 19, Damping Coefficient and Spring Constant Comparison for Tuning Methods

These findings show that, although the classical tuning method provides improved system damping response to coning motions, optimization can achieve much better results. Using exact, linear equations of motion, optimization schemes are created which are useful over all stable regions of the parameters given. On the contrary, classical tuning methods are not applicable for small values of the spring constant, k . Due to an extreme sensitivity of the damping rate to the spring constant in classical methods, any slight deviations in selection of the spring constant through Equation 27 could lead to unsatisfactory results. These slight discrepancies come as a result of the limitations in selecting an arbitrary, small damping coefficient. By using optimization schemes, the nutation damper designer can

obtain exact values for the damping coefficient and spring constant, limited only by the optimization algorithm itself.

Optimization of the exact, linearized equations of motion allows the satellite nutation damper designer to obtain values for the system parameters which maximize the rate of damping. The classical tuning method, in which the rigid body and spring-mass-damper are decoupled, provides a parameter set yielding inferior results. This chapter shows that optimization provides results which are more precise and promote faster damping rates.

VI. Conclusion

Designers have realized the need for good nutation damper designs over the course of spacecraft evolution. Efficient passive attitude control mechanisms are critical to providing simpler, less costly mission support. Spin-stabilized satellites in particular are key prospects for the incorporation of nutation dampers to control coning motion. This satellite "wobble" may be caused by external perturbations such as crew movement, booster separation, docking, or magnetic torques. A nutation damper, acting as the energy dissipation device, returns the satellite's angular momentum vector to an alignment with its spin axis. In doing so, the satellite remains pointed to accomplish its designed mission.

The study of a rigid body with an attached spring-mass-damper has often coincided with satellite research. While many of the stability analyses of these systems were developed during the 1960s, designs eventually shifted toward more complicated, costly control schemes. Historically, only approximate solutions have existed in discussions of nutation dampers and studies have been limited to estimates on their designs. In classical damper design, the mathematically uncoupled rigid body frequency is equated, or tuned, to that of the spring-mass-damper. While this method has been shown to improve the cone angle decay response, it is not truly an optimal solution.

With the non-dimensional equations of motion, an analysis of the eigenvalues leads to a stability analysis of the system. Based upon the eigenvalue response, the spring-mass-damper can damp out critically while the rigid body cannot. To achieve favorable

damping conditions, the damping rate is optimized by maximizing the magnitude of the real part of the stable, rigid body eigenvalues.

A study of individual parameters which describe the symmetry, I_1 and I_3 , the mass fraction, ϵ , damper placement, b , damping coefficient, c , and spring constant, k , illustrates their independent effects. The moments of inertia, I_1 and I_3 , have a noticeable effect on the performance of the nutation damper. A relatively asymmetric rigid body provides a greater damping rate, and when $I_1 > I_3$, a much improved damping rate is seen. This phenomenon is expected since the nutation damper studied has a single degree of freedom. When increased, the mass fraction, ϵ , provides a greater damping response to coning as well. As the damper placement, b , increases, the damping rate also increases due to the torque applied to the rigid body. Since the effects of I_1 , I_3 , ϵ , and b appear to be independent, they are fixed in the optimization function, leaving only the damping coefficient, c , and spring constant, k , as variable parameters. Results show that for small c and k , the damper provides favorable response to coning. As the damping increases, the system becomes overdamped and when the spring constant increases, the system becomes underdamped. This result illustrates that the damping coefficient and spring constant are somewhat proportional.

Optimization reduces to maximizing the damping rate by minimizing the real eigenvalue parts of the rigid body. Only c and k are allowed as optimization variables, although the effects of b are depicted. It is seen that optimal damping response occurs only for small values of c and k , while verifying that the two are almost linearly related for non-optimal regions.

By comparing the rigid body and spring-mass-damper eigenvalues at optimum, the two pairs approach equality. Initially, classical tuning methods, which equate the two frequencies, seem to be correct. However, it is clear that an optimized solution is capable of producing a remarkable improvement in damping rates. In classical methods, a slight deviation in parameter selection leads to marked differences in performance. On the contrary, optimal solutions offer an exact result which yield the greatest attainable damping rate for the decay of coning. The solutions presented here can be modified to fit other satellite models and may provide satellite attitude control system designers with improved performance of simple, passive nutation dampers attached to spin-stabilized satellites.

Appendix A: Sample MatLab Code

```

%%
%%
%% This code defines constants, then solves for values of c which
%% impart the minimum real eigenvalue part over a range of k =
%% {0.002, 0.004}. It must be used in conjunction with the
%% function F(c).
%%
%% The optimization tolerance of fmin may be defined as 10-10 by:
%%     fmin('F',cmin,cmax,[0,10^(-10)])
%%
%% Similarly, the fmins function can be used to solve for multiple
%% variables by invoking:
%%     fmins('MinFn',[guess1,guess2],[0,10^(-10)])
%%
%%

```

```

%e = ε, ep = ε'
e=0.01;
ep=1-e;
I3=0.7;
I1=0.6;
b = 3;
B = b*e - ep*I3;
j = 0;

```

```

%cmin and cmax define range of search
cmin = 0;
cmax=0.02;

```

```

Vals = zeros(100,2);
for k = 0.002:0.00002:0.004
    j=j+1;

```

```

    %Find c which yields minimum real eigenvalue (= ans)
    fmin('F',cmin,cmax);
    Min=F(ans);
    Vals(j,:) = [k Min];

```

```

end

```

```

%% %% %% %% %% %% %% %% %% %% %% %% %% %% %% %% %% %% %% %% %% %% %% %% %%
%
% This function defines 'F' as a routine which will return the %
% value for c which results in the minimum real eigenvalue part. %
% It must be used in conjunction with a statement resembling: %
% fmin('F',cmin,cmax) %
% %
% Where [cmin,cmax] = range of acceptable values for c. %
% %
%% %% %% %% %% %% %% %% %% %% %% %% %% %% %% %% %% %% %% %% %% %% %% %% %%

```

```

function minev = F(c)
global k b e ep I3 I1;

M = [ 0 -1+ep/(-(b*e)+ep*I3) -(b/(-(b*e)+ep*I3)) 0;
      (-1+I1)/I1 0 0 -(b*e/I1);
      -(e/I1) c/(-(b*e)+ep*I3) -c*I3/(e*(-(b*e)+ep*I3)) -(b*e^2/I1)-k;
      0 -(1/(-(b*e)+ep*I3)) I3/(e*(-(b*e)+ep*I3)) 0 ];

evals = eig(M);
[minev,imin] = min(real(evals(:,1)));

```

```

%% %% %% %% %% %% %% %% %% %% %% %% %% %% %% %% %% %% %% %% %% %% %%
%
% This function defines 'MinFn' as a routine which will return
% values for c and k which yield the minimum real eigenvalue part.
% It may be used in conjunction with the statement
% fmins('MinFn',[guess1, guess2])
%
% Where [guess1,guess2] = initial estimates of c and k.
%
%% %% %% %% %% %% %% %% %% %% %% %% %% %% %% %% %% %% %% %% %% %% %%

```

```
function minev = MinFn(v)
```

```
global e ep I3 I1 b;
```

```
c=v(1);
```

```
k=v(2);
```

```

M = [ 0 -1+ep/(-(b*e)+ep*I3) -(b/(-(b*e)+ep*I3)) 0;
      (-1+I1)/I1 0 0 -(b*e/I1);
      -(e/I1) c/(-(b*e)+ep*I3) -c*I3/(e*(-(b*e)+ep*I3)) -(b*e^2/I1)-k;
      0 -(1/(-(b*e)+ep*I3)) I3/(c*(-(b*c)+ep*I3)) 0 ];

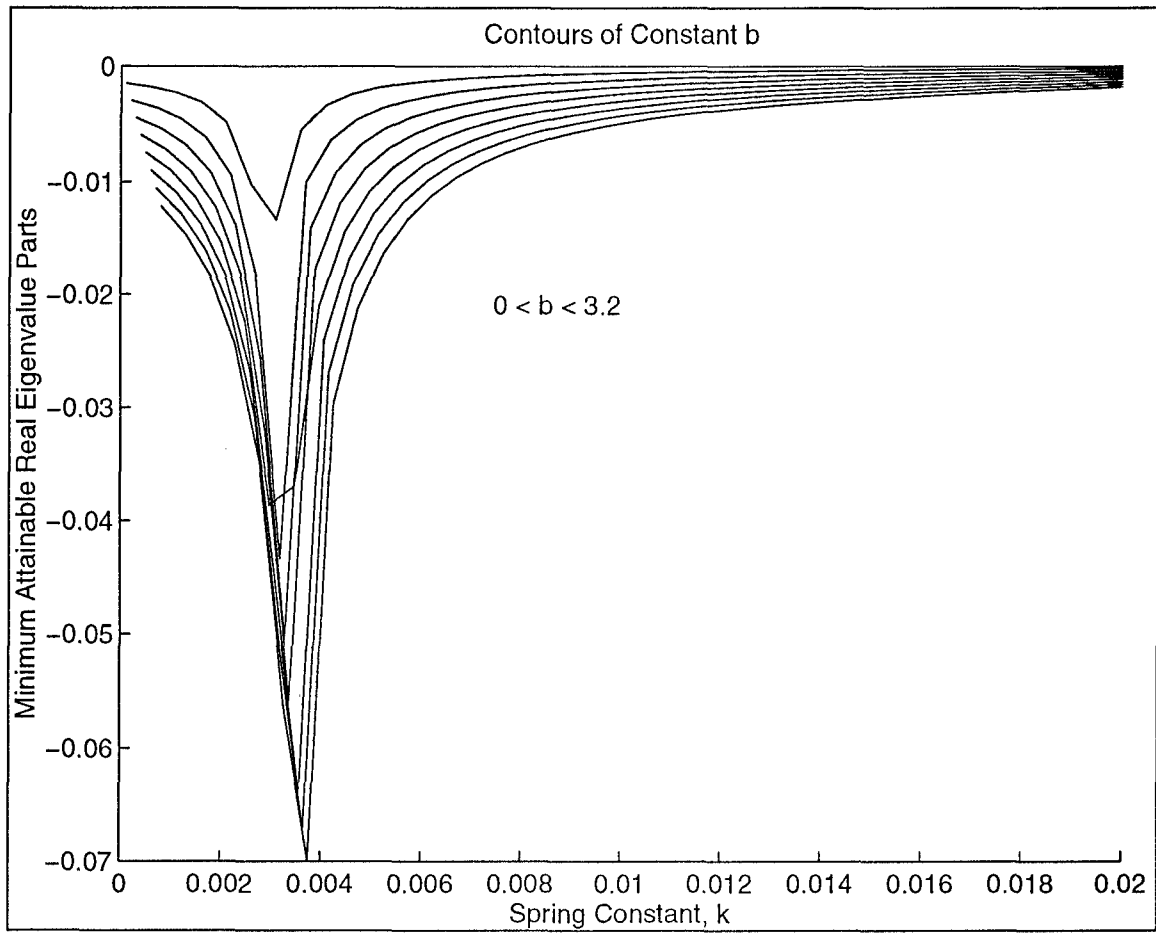
```

```
evals = eig(M);
```

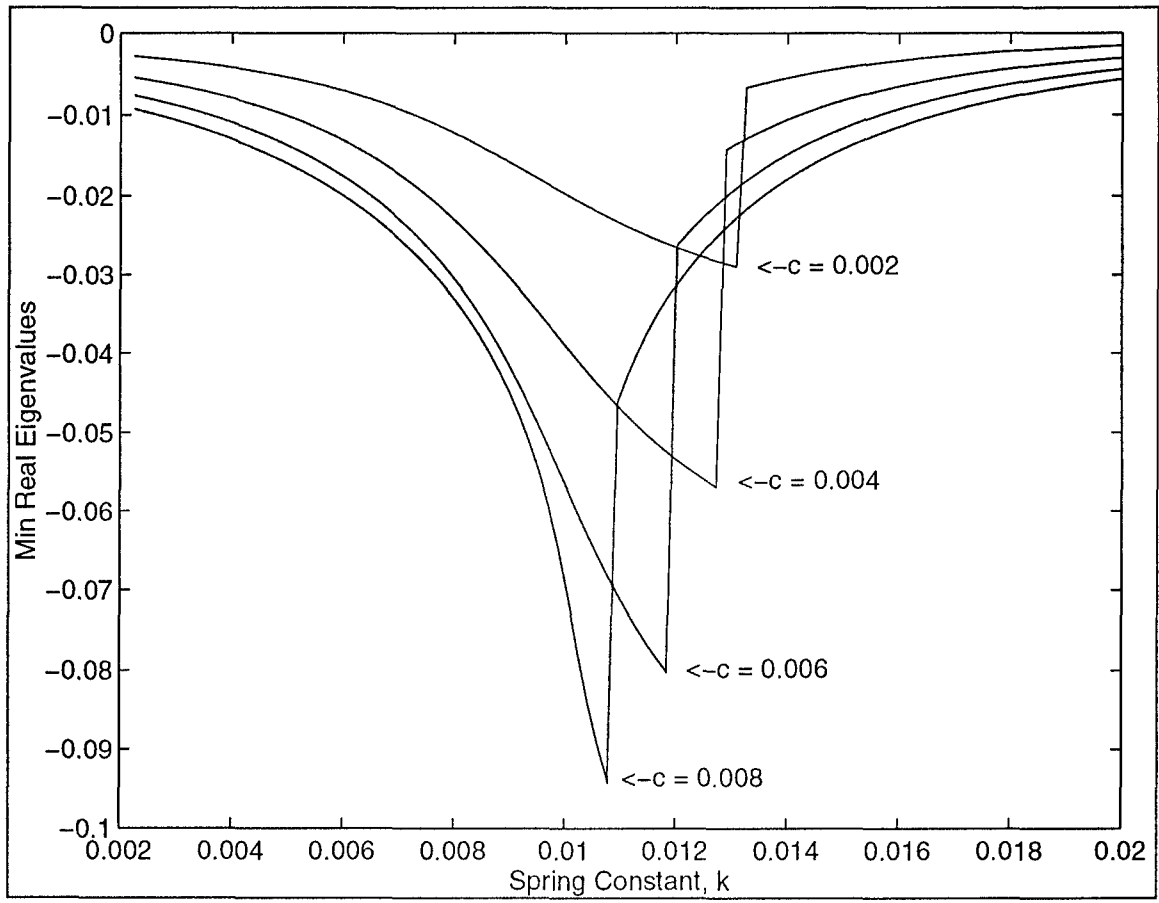
```
[minev,imin] = min(real(evals(:,1)));
```


Appendix B: Supportive Plots

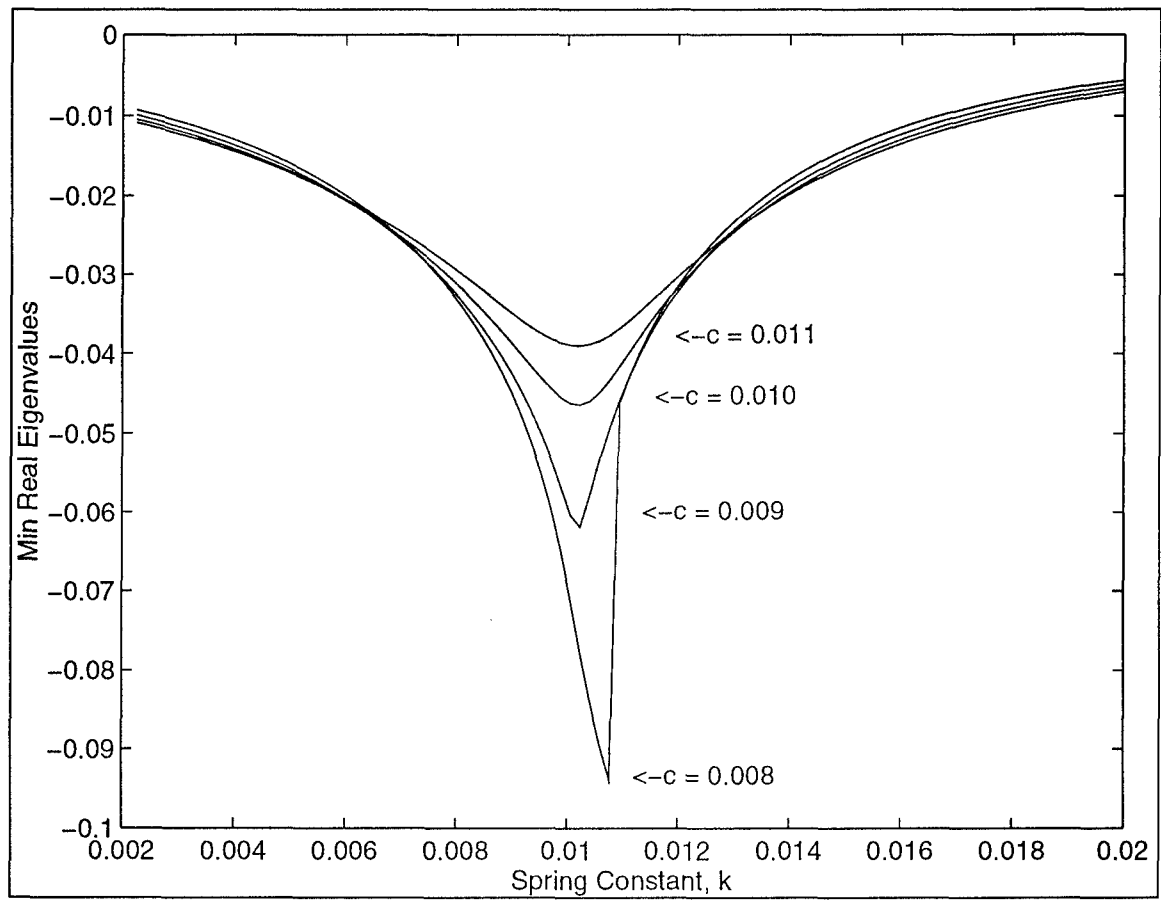
Effect of Increasing b on the magnitude of the damping rate



Effect of Increasing c to 0.008

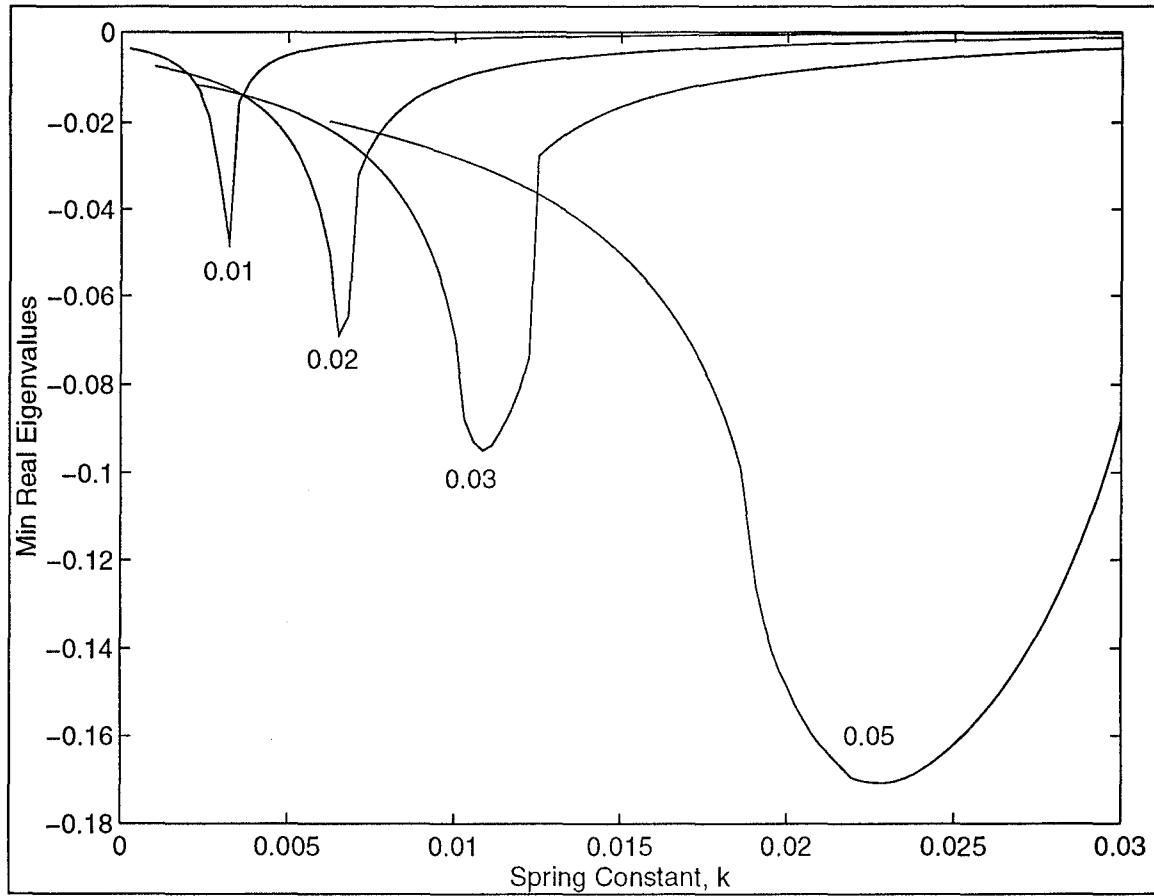


Effect of Increasing c from 0.008 to 0.011

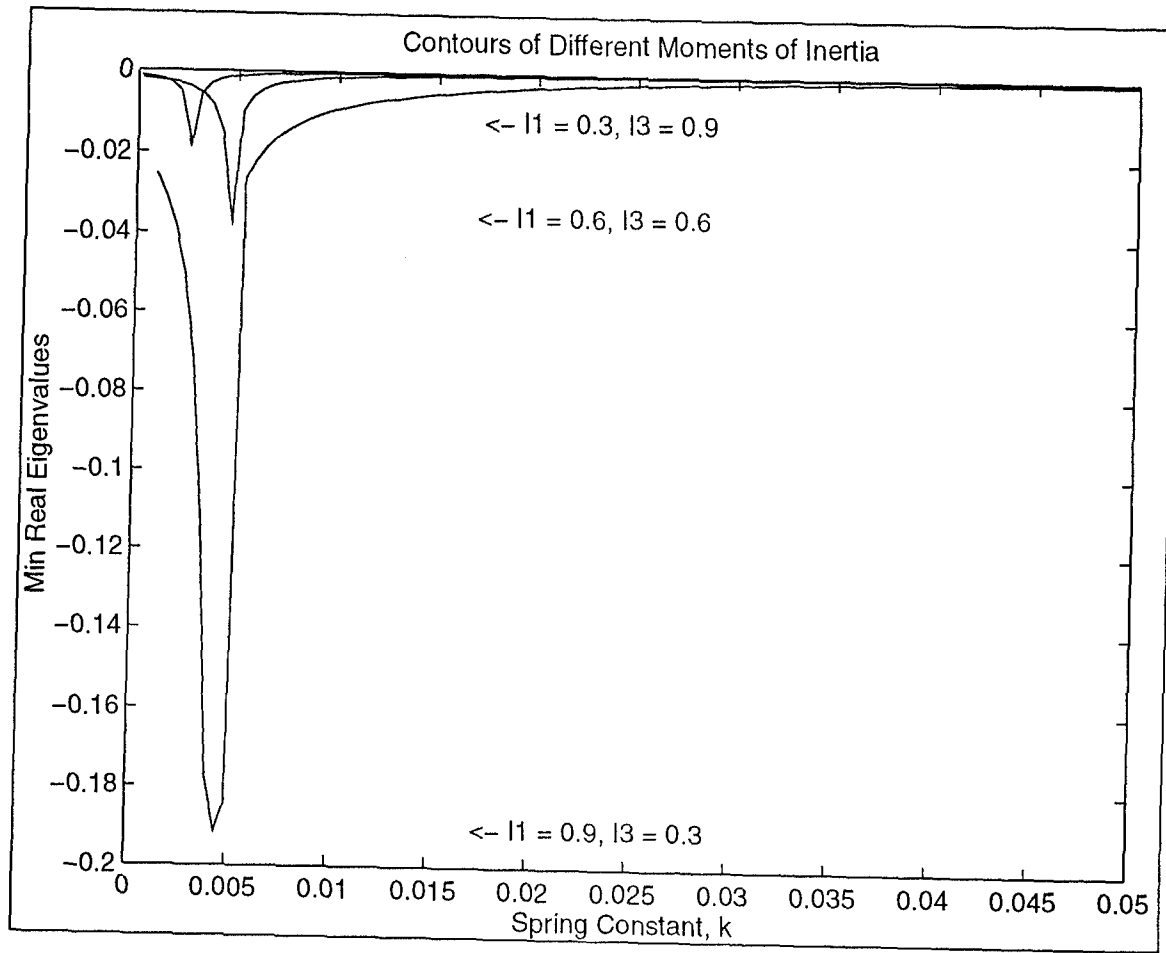


Effect of Increasing the Mass Fraction

Note that the optimal area increases with ϵ



Effects of Several Combinations of the Moments of Inertia



Bibliography

1. Alfriend, Kyle T. "Partially Filled Viscous Ring Nutation Damper." Journal of Spacecraft and Rockets. Vol. 11, No. 7. July, 1974. pp. 456-462.
2. Alper, J. R. "Analysis of Pendulum Damper for Satellite Wobble Damping." Journal of Spacecraft and Rockets. Vol. 2, No. 1. January-February, 1965. pp. 50-54.
3. Austin, Fred, and Zetkov, George A. "Zero Mass-Shift Passive Damper for the Reduction of Precession in a Rotating Space Vehicle." Journal of the Astronautical Sciences. Vol. 16, No. 1. January-February, 1969. pp. 1-7.
4. Bhuta, P. G., and Koval, L. R. "A Viscous Ring Damper for a Freely Precessing Satellite." International Journal of Mechanical Sciences. Vol. 8. 1966. pp. 383-395.
5. Borelli, R. L., and Leliakov, I. P. "An Optimization Technique for the Transient Response of Passively Stable Satellites." Journal of Optimization Theory and Applications. Vol. 10, No. 6. 1972. pp. 344-361.
6. Chang, C. O., and Wang, I. P. "Analysis of a Nutation Damper for a Two-Degree of Freedom Gyroscope." Journal of Guidance, Control, and Dynamics. Vol. 15, No. 1. January-February, 1992. pp. 165-174.
7. Chinnery, Anne C., and Hall, Christopher D. "The Motion of a Rigid Body with an Attached Spring-Mass-Damper." Proceedings of the AIAA/AASS 1994 Astrodynamics Conference. Scottsdale AZ. August, 1994. pp. 74-81.
8. Chinnery, Anne C. Numerical Analysis of the Motion of a Rigid Body with an Attached Spring-Mass-Damper. MS Thesis, AFIT/GAE/ENY/93D-8. Graduate School of Engineering, Air Force Institute of Technology (AETC), Wright-Patterson AFB OH. December, 1993. (AD-A273825).
9. Cloutier, Gerald J. "Nutation Damper Instability on Spin-Stabilized Spacecraft." AIAA Journal. Vol. 7, No. 11. November, 1969. pp. 2110-2115.
10. Cochran, J. E., and Thompson, J. A. "Nutation Dampers vs. Precession Dampers for Asymmetric Spacecraft." Journal of Guidance, Control, and Dynamics. Vol. 3, No. 1. January-February, 1980. pp. 22-28.
11. Craig, B. D. "Nutation Damper for OSO." Astronautics and Aerospace Engineering. Vol. 1, No. 11. December, 1963. pp. 50-55.

12. Etkin, B. "Dynamics of Gravity-Oriented Orbiting Systems With Application to Passive Stabilization." AIAA Journal. Vol. 2, No. 6. June, 1964. pp. 1008-1014.
13. Haseltine, W. R. "Nutation Damping Rates for a Spinning Satellite." Aerospace Engineering. March, 1962. pp. 10-16.
14. -----, "Passive Damping of Wobbling Satellites: General Stability Theory and Example." Journal of the Aerospace Sciences. Vol. 29, No. 5. May, 1992. pp. 543-550.
15. Hughes, Peter C. Spacecraft Attitude Dynamics. New York: John Wiley and Sons, 1986.
16. Kane, Thomas R., and Levinson, David A. "A Passive Method for Eliminating Coning of Force-Free, Axisymmetric Rigid Bodies." Journal of the Astronautical Sciences. Vol. 40, No. 10. October-December, 1992. pp. 439-447.
17. Likins, Peter W. Elements of Engineering Mechanics. New York: McGraw-Hill, Inc., 1973.
18. Math Works, Inc. Pro-MatLab User's Guide. South Natick NJ. 31 January 1990.
19. Milman, Mark H., and Chu, Cheng-Chih. "Optimization Methods for Passive Damper Placement and Tuning." Journal of Guidance, Control, and Dynamics. Vol. 17, No. 4. July-August, 1994. pp. 848-856.
20. Sarychev, V. A., and Sazonov, V. V. "Spin-Stabilized Satellites." Journal of the Astronautical Sciences. Vol. 24, No. 4. October-December, 1976. pp. 291-310.
21. Schneider, C. C., Jr., and Likins, P. W. "Nutation Dampers vs. Precession Dampers for Asymmetric Spinning Spacecraft." Journal of Spacecraft and Rockets. Vol. 10, No. 3. March, 1973. pp. 218-222.
22. Shabana, A. A. Theory of Vibration. Volume I: An Introduction. New York: Springer-Verlag, 1990.
23. Taylor, Robert S. "A Passive Pendulum Wobble Damping System for a Manned Rotating Space Station." Journal of Spacecraft and Rockets. Vol. 3, No. 8. August, 1966. 1221-1228.
24. Wadleigh, K. H., Galloway, A. J., and Mathur, P. N. "Spinning Vehicle Nutation Damper." Journal of Spacecraft and Rockets. Vol. 1, No. 6. November-December, 1964. pp. 588-592.
25. Wiesel, William E. Spaceflight Dynamics. New York: McGraw-Hill, Inc., 1989.

26. Yu, E. Y. "Spin Decay, Spin-Precession Damping, and Spin-Axis Drift of the *Telstar* Satellite." Bell System Technical Journal. Vol. 42, No. 5. September, 1963. pp. 2169-2193.
27. MatLab. Version 4.2a, SPARC. Computer Software. The MathWorks, Inc., South Natick NJ. May 13, 1994.
28. Mathematica. Version 2.0, SPARC. Computer Software. Wolfram Research, Inc., 1991.

Vita

Second Lieutenant Brady P. Hauboldt was born September 20, 1970, in Wausau, Wisconsin. He graduated in 1989 from D. C. Everest Senior High School in Schofield, Wisconsin, and entered undergraduate studies at the United States Air Force Academy in Colorado Springs, Colorado. In June of 1993, he graduated with a Bachelor of Science degree in Engineering Mechanics and was commissioned. In July of the same year, he entered the Graduate School of Engineering, Air Force Institute of Technology, in Dayton, Ohio.

Permanent Address: 2183 River Forest Lane
 Mosinee, WI 54455

REPORT DOCUMENTATION PAGE

Form Approved
OMB No. 0704-0188

Public reporting burden for this collection of information is estimated to average 1 hour per response, including the time for reviewing instructions, searching existing data sources, gathering and maintaining the data needed, and completing and reviewing the collection of information. Send comments regarding this burden estimate or any other aspect of this collection of information, including suggestions for reducing this burden, to Washington Headquarters Services, Directorate for Information Operations and Reports, 1215 Jefferson Davis Highway, Suite 1204, Arlington, VA 22202-4302, and to the Office of Management and Budget, Paperwork Reduction Project (0704-0188), Washington, DC 20503.

1. AGENCY USE ONLY (Leave blank)	2. REPORT DATE December 1994	3. REPORT TYPE AND DATES COVERED Master's Thesis	
4. TITLE AND SUBTITLE OPTIMIZATION OF A NUTATION DAMPER ATTACHED TO A SPIN-STABILIZED SATELLITE		5. FUNDING NUMBERS	
6. AUTHOR(S) Brady P. Hauboldt, 2LT, USAF		7. PERFORMING ORGANIZATION NAME(S) AND ADDRESS(ES) Air Force Institute of Technology Wright-Patterson AFB, OH 45433-6583	
8. PERFORMING ORGANIZATION REPORT NUMBER AFIT/GSO/ENY/94D-2		9. SPONSORING/MONITORING AGENCY NAME(S) AND ADDRESS(ES) PL/VTA (Captain Nathan Titus) 3550 Aberdeen Ave SE Kirtland AFB, NM 87117	
10. SPONSORING/MONITORING AGENCY REPORT NUMBER		11. SUPPLEMENTARY NOTES	
12a. DISTRIBUTION/AVAILABILITY STATEMENT Approved for public release; distribution unlimited		12b. DISTRIBUTION CODE	
13. ABSTRACT (Maximum 200 words) This study uses linearized equations of motion for a rigid body with an attached spring-mass-damper to maximize the decay rate of a satellite's coning motion. An analysis of the numerical eigenvalues is presented which leads to an optimal relationship between relevant parameters: damper placement, spring constant, damping coefficient, system moments of inertia, and damper mass fraction. The coupled system's eigenvalues do not provide truly critical damping, thus the real eigenvalue parts are minimized in order to achieve damping which requires the minimum amount of time. A comparison between this optimal design method and a classical method concludes a noticeable improvement in damping performance for optimized systems.			
14. SUBJECT TERMS Nutation Dampers; Satellite Stability; Damper Tuning Damper Optimization			15. NUMBER OF PAGES 66
16. PRICE CODE			17. SECURITY CLASSIFICATION OF REPORT Unclassified
18. SECURITY CLASSIFICATION OF THIS PAGE Unclassified	19. SECURITY CLASSIFICATION OF ABSTRACT Unclassified	20. LIMITATION OF ABSTRACT UL	